PHYSICAL REVIEW D **74,** 064011 (2006)

Circular orbits and spin in black-hole initial data

Matthew Caudill,* Gregory B. Cook,† and Jason D. Grigsby‡
Department of Physics, Wake Forest University, Winston-Salem, North Carolina 27109, USA

Harald P. Pfeiffer§
Theoretical Astrophysics, California Institute of Technology, Pasadena, California 91125, USA
(Received 9 May 2006; published 11 September 2006)

The construction of initial data for black-hole binaries usually involves the choice of free parameters that define the spins of the black holes and essentially the eccentricity of the orbit. Such parameters must be chosen carefully to yield initial data with the desired physical properties. In this paper, we examine these choices in detail for the quasiequilibrium method coupled to apparent-horizon/quasiequilibrium boundary conditions. First, we compare two independent criteria for choosing the orbital frequency, the ''Komar-mass condition'' and the ''effective-potential method,'' and find excellent agreement. Second, we implement quasilocal measures of the spin of the individual holes, calibrate these with corotating binaries, and revisit the construction of *nonspinning* black-hole binaries. Higher-order effects, beyond those considered in earlier work, turn out to be important. Without those, supposedly nonspinning black holes have appreciable quasilocal spin; furthermore, the Komar-mass condition and effective-potential method agree only when these higher-order effects are taken into account. We compute a new sequence of quasicircular orbits for nonspinning black-hole binaries, and determine the innermost stable circular orbit of this sequence.

DOI: 10.1103/PhysRevD.74.064011 PACS numbers: 04.20.−q, 04.25.Dm, 04.70.Bw, 97.80.−d

I. INTRODUCTION

Recently, significant progress has been made in numerically evolving black-hole binaries [1–4]. A major goal of these simulations is to estimate the gravitational waveform produced by astrophysical black-hole binaries. These waveforms will ultimately be used to aid in the detection and interpretation of the gravitational wave signals we expect to see in observatories such as LIGO, VIRGO, TAMA, and GEO600. In order for such simulations to yield astrophysically relevant results, the initial data must be constructed to be astrophysically realistic.

A very effective approach for constructing numerical black-hole binary initial data has been developed and explored by two of the authors [5] (see also Refs. [6–8]). In Ref. [5], the authors focused attention on two specific, limiting cases of binary initial data: corotating black holes and irrotational (nonspinning) black holes. These numerical initial-data solutions were compared against previous numerical results [8,9] and to analytic post-Newtonian estimates [10,11] for binaries in circular orbits and appear to give the best agreement yet between numerical and analytic models of close black-hole binaries in circular orbits. However, various aspects of the physical content of these initial-data sets have not been fully tested.

In order to construct quasicircular orbits (as opposed to general elliptical orbits), Gourgoulhon *et al.* [7] proposed that the data must satisfy a simple condition: the Komar [12] and the ADM [13] masses must agree if the orbits are quasicircular. The Komar mass is only a reasonable definition of the total mass of a system if the system is *stationary*. The ADM mass is an invariant measure of the total mass of a system as measured at spacelike infinity. So, for binary systems that are quasistationary when they are in quasicircular orbit, the ansatz seems quite reasonable. This ansatz has been tested by comparing numerical models with analytic post-Newtonian models. It has also been tested in the case of neutron-star binaries [14] where an independent method of determining circular orbits exists. For black-hole binaries, an independent method of determining circular orbits exists in the so-called *effective-potential method* [9]. In this paper, we will further test the Komar-ADM mass ansatz by constructing circular orbits using the effective-potential method.

Another important aspect of the binary initial data constructed in Ref. [5] that has not been adequately verified relates to the spins of the individual black holes. In Ref. [5], the spin of each black hole is fixed by a particular choice of boundary conditions applied at the surface of the black hole. For the case of corotating black holes, the choice of boundary conditions is unambiguous. However, for nonspinning black holes, the boundary conditions were chosen in a way that should be correct in the limit of large separation between the black holes in the binary. However, this nonspinning ansatz has not yet been checked.

Of course, we must keep in mind that the angular momentum (spin) of an individual black hole in a close

*Current address: Department of Physics, Washington University in St. Louis, St. Louis, Missouri 63130. Electronic address: mscaudil@artsci.wustl.edu
†Electronic address: cookgb@wfu.edu
‡Electronic address: grigjd3@wfu.edu
§Electronic address: harald@tapir.caltech.edu

binary system is not rigorously defined in general relativity. To measure the spin, we will have to rely on a quasilocal definition. There are many such definitions [15]. For our purposes, we will use a definition first made rigorous by Brown and York [16] and also derived within the more recent *isolated horizons* framework of Ashtekar and Krishnan [17,18]. We will explore extensively the spins of the individual black holes in our binary initial data using this quasilocal definition of the angular momentum. A major result of this study is that we must refine our method for setting the boundary conditions in order to construct models where the black holes are not rotating.

We begin in Sec. II with a review of the entire formalism used to construct our initial data. In Sec. III we discuss various issues associated with computing the quasilocal spin of a black hole. In Sec. IV we examine the case of corotating binaries, focusing first on exploring the criteria for defining circular orbits and then examining the spins of corotating black holes. In Sec. V we turn to the case of nonspinning binaries and define the correct approach for obtaining nonspinning black holes. Finally, in Sec. VI we present results related to the innermost stable circular orbits for both nonspinning and corotating binaries, and review the major points from the paper.

II. INITIAL-DATA FORMALISM

The black-hole initial-data sets that we consider below are constructed using the conformal thin-sandwich decomposition [19,20], a set of boundary conditions imposed on the black-hole excision surfaces [5,6] and at asymptotic infinity, and a set of assumptions for various freely specifiable fields. Below, we will outline the most important details of the various pieces of our approach.

A. The conformal thin-sandwich decomposition

In this work, we will use the standard 3 + 1 decomposition with the interval written as

$$\mathrm{d}s^2 = -\alpha \mathrm{d}t^2 + \gamma_{ij}(\mathrm{d}x^i + \beta^i \mathrm{d}t)(\mathrm{d}x^j + \beta^j \mathrm{d}t), \quad (1)$$

where γ_{ij} is the 3-metric induced on a $t =$ const spatial hypersurface, α is the lapse function, and β^i is the shift vector. The extrinsic curvature of the spatial slice, K_{ij}, is defined by

$$K_{\mu\nu} \equiv -\tfrac{1}{2}\gamma^{\delta}_{\mu}\gamma^{\rho}_{\nu}\mathcal{L}_n \gamma_{\delta\rho}, \quad (2)$$

where $\mathcal{L}_n$ denotes the Lie derivative along the unit normal to the spatial slice, n^μ. Einstein's equations, in vacuum, then reduce to four sets of equations. Two are evolution equations for the spatial metric and extrinsic curvature:

$$\partial_t \gamma_{ij} = -2\alpha K_{ij} + 2\nabla_{(i}\beta_{j)}, \quad (3)$$

and

$$\partial_t K_{ij} = -\nabla_i \nabla_j \alpha + \alpha[R_{ij} - 2K_{i\ell}K^{\ell}_{j} + KK_{ij}] + \beta^{\ell}\nabla_{\ell}K_{ij} + 2K_{\ell(i}\nabla_{j)}\beta^{\ell}. \quad (4)$$

The remaining two are the constraint equations

$$R + K^2 - K_{ij}K^{ij} = 0 \quad (5)$$

and

$$\nabla_j(K^{ij} - \gamma^{ij}K) = 0. \quad (6)$$

Here, ∇_i, R_{ij}, and R are, respectively, the covariant derivative, Ricci tensor, and Ricci scalar associated with the spatial metric γ_{ij}. Finally, the trace of the extrinsic curvature is denoted $K \equiv K^i_i$.

The conformal thin-sandwich decomposition employs a York-Lichnerowicz conformal decomposition of the metric and various other quantities [21–23]. The conformal factor, ψ, is defined via

$$\gamma_{ij} \equiv \psi^4 \tilde{\gamma}_{ij}, \quad (7)$$

where $\tilde{\gamma}_{ij}$ is a "conformal metric." The time derivative of the conformal metric is introduced by the definitions

$$\tilde{u}_{ij} \equiv \partial_t \tilde{\gamma}_{ij}, \quad (8)$$

$$\tilde{\gamma}^{ij}\tilde{u}_{ij} \equiv 0. \quad (9)$$

From this, it follows that the tracefree extrinsic curvature $A^{ij} \equiv K^{ij} - \frac{1}{3}\gamma^{ij}K$ takes the form

$$A^{ij} = \frac{\psi^{-10}}{2\tilde{\alpha}}[(\tilde{\mathbb{L}}\beta)^{ij} - \tilde{u}^{ij}], \quad (10)$$

where $\tilde{\alpha} \equiv \psi^{-6}\alpha$ is the conformal lapse function, and $\tilde{u}^{ij} = \tilde{u}_{kl}\tilde{\gamma}^{ik}\tilde{\gamma}^{jl}$. Furthermore, $(\tilde{\mathbb{L}}V)$ is the conformal-Killing (or longitudinal) operator acting on a vector, defined by

$$(\tilde{\mathbb{L}}V)_{ij} \equiv 2\tilde{\nabla}_{(i}V_{j)} - \tfrac{2}{3}\tilde{\gamma}_{ij}\tilde{\nabla}_k V^k, \quad (11)$$

where $\tilde{\nabla}_k$ is the covariant derivative compatible with $\tilde{\gamma}_{ij}$. Finally, the conformal tracefree extrinsic curvature can be written as

$$\tilde{A}^{ij} \equiv \psi^{10}A^{ij} = \frac{1}{2\tilde{\alpha}}[(\tilde{\mathbb{L}}\beta)^{ij} - \tilde{u}^{ij}]. \quad (12)$$

In terms of our conformally decomposed variables, the Hamiltonian constraint (5) can be written

$$\tilde{\nabla}^2\psi - \frac{1}{8}\psi\tilde{R} - \frac{1}{12}\psi^5 K^2 + \frac{1}{8}\psi^{-7}\tilde{A}_{ij}\tilde{A}^{ij} = 0, \quad (13)$$

where $\tilde{R}$ is the Ricci scalar associated with $\tilde{\gamma}_{ij}$, and the momentum constraint (6) as

$$\tilde{\nabla}_j\left(\frac{1}{2\tilde{\alpha}}(\tilde{\mathbb{L}}\beta)^{ij}\right) - \frac{2}{3}\psi^6\tilde{\nabla}^i K - \tilde{\nabla}_j\left(\frac{1}{2\tilde{\alpha}}\tilde{u}^{ij}\right) = 0. \quad (14)$$

Furthermore, the trace of Eq. (4) can be written as

$$\tilde{\nabla}^2(\psi^7\tilde{\alpha}) - (\psi^7\tilde{\alpha})\left(\frac{1}{8}\tilde{R} + \frac{5}{12}\psi^4K^2 + \frac{7}{8}\psi^{-8}\tilde{A}_{ij}\tilde{A}^{ij}\right) = -\psi^5(\partial_t K - \beta^k\tilde{\nabla}_k K). \quad (15)$$

Within the conformal thin-sandwich formalism, the fundamental variables are: ψ, $\tilde{\alpha}$, β^i, $\tilde{\gamma}_{ij}$, K, $\partial_t\tilde{\gamma}_{ij} \equiv \tilde{u}_{ij}$, and $\partial_t K$. Of these, $\tilde{\gamma}_{ij}$, K, $\tilde{u}_{ij}$, and $\partial_t K$ represent the eight gauge and dynamical degrees of freedom of the gravitational field. These fields must be chosen based on the physics of the initial data one wishes to model. The remaining fields, ψ, $\tilde{\alpha}$, and β^i, represent the constrained degrees of freedom. Once the other fields have been fixed, these fields are determined by solving Eqs. (13)–(15) as a set of coupled elliptic equations.

Formulating a well-posed elliptic system requires that we impose boundary conditions. Typically, these systems are solved under the assumption that the spacetime is asymptotically flat. If we let r denote a coordinate radius measured from the location of the center of energy of the system, then as $r \to \infty$ we have that

$$\psi|_{r\to\infty} = 1, \quad (16a)$$

$$\beta^i|_{r\to\infty} = (\mathbf{\Omega}_0 \times \mathbf{r})^i, \quad (16b)$$

$$\alpha|_{r\to\infty} = \tilde{\alpha}|_{r\to\infty} = 1. \quad (16c)$$

Ω_0 is the orbital angular velocity of a binary system, or the rotational angular velocity of a single object, as measured at infinity. The boundary condition on the shift is chosen so that the time coordinate, $t^\mu = \alpha n^\mu + \beta^\mu$, is helical and tracks the rotation of the system [5–7,24,25]. If we wish to consider systems with one or more black holes, and if we excise the interior of the black hole to avoid difficulties with singularities, then we must also impose boundary conditions on the excision surfaces.

B. Black-hole excision boundary conditions

In this paper, we are interested in the situation in which each black hole is in quasiequilibrium and the boundary conditions required to achieve this were worked out in Refs. [5,6]. The assumptions are essentially the same as those required of an "isolated horizon" (cf. [17,26–28]). To ensure that the black hole is in quasiequilibrium, we enforce the following conditions. First, we demand that the expansion θ, of the outgoing null rays, k^μ, vanishes on the excision surface, $\mathcal{S}$, thus forcing the boundary to be an apparent horizon:

$$\theta|_{\mathcal{S}} = 0. \quad (17)$$

Next, we require that the shear $\sigma_{\mu\nu}$ of the outgoing null rays also vanish on the excision boundary,

$$\sigma_{\mu\nu}|_{\mathcal{S}} = 0. \quad (18)$$

In the absence of matter on $\mathcal{S}$, Eqs. (17) and (18) are sufficient to imply that

$$\mathcal{L}_k\theta|_{\mathcal{S}} = 0. \quad (19)$$

That is, initially, the apparent horizon will evolve along k^μ.

Conditions (17)–(19) are coordinate independent, however the final demand breaks precisely this coordinate freedom. This final condition is that the *coordinate location* of the apparent horizon does not move initially in an evolution of the initial data. Let the excision boundary surface, $\mathcal{S}$, be a spacelike 2-surface with topology S^2 and define s^i to be the outward pointing unit vector normal to the surface. If we let

$$k^\mu \equiv \frac{1}{\sqrt{2}}(n^\mu + s^\mu) \quad (20)$$

represent the set of outgoing null rays associated with $\mathcal{S}$, and with the time vector written as

$$t^\mu = \alpha n^\mu + \beta^\mu, \quad (21)$$

then this condition can be expressed as

$$t^\mu k_\mu|_{\mathcal{S}} = 0. \quad (22)$$

This immediately yields

$$\alpha|_{\mathcal{S}} = \beta^i s_i|_{\mathcal{S}}. \quad (23)$$

To further analyze Eq. (23), we split the shift vector into its component normal to the surface, $\beta_\perp$, and a vector tangent to the surface, $\beta_\parallel{}^i$, defined by

$$\beta_\perp \equiv \beta^i s_i, \quad (24)$$

$$\beta_\parallel{}^i \equiv h^i_j\beta^j, \quad (25)$$

where $h_{ij} \equiv \gamma_{ij} - s_i s_j$ is the metric induced on $\mathcal{S}$ by γ_{ij}. We see that Eq. (23) is a condition on the normal component of the shift,

$$\beta_\perp|_{\mathcal{S}} = \alpha|_{\mathcal{S}}. \quad (26)$$

The conformal transformation on γ_{ij}, Eq. (7), induces a natural conformal weighting for h_{ij} and for the unit normal to $\mathcal{S}$,

$$h_{ij} \equiv \psi^4\tilde{h}_{ij}, \quad (27)$$

$$s^i \equiv \psi^{-2}\tilde{s}^i. \quad (28)$$

In terms of these conformal quantities, the condition in Eq. (17) takes the form of a nonlinear Robin-type boundary condition on the conformal factor ψ,

$$\tilde{s}^k\tilde{\nabla}_k \ln\psi|_{\mathcal{S}} = -\frac{1}{4}\left(\tilde{h}^{ij}\tilde{\nabla}_i\tilde{s}_j + \frac{K}{6}\psi^2 - \frac{\psi^{-4}}{8\tilde{\alpha}}\tilde{s}_i\tilde{s}_j[(\tilde{\mathbb{L}}\beta)^{ij} - \tilde{u}^{ij}]\right)\Big|_{\mathcal{S}}. \quad (29)$$

We now turn our attention to Eq. (18), which can be rewritten as

$$\tilde{D}^{(i}{\beta_\parallel}^{j)}|_{\mathcal{S}} - \tfrac{1}{2}\tilde{h}^{ij}\tilde{D}_k{\beta_\parallel}^k|_{\mathcal{S}} = \tfrac{1}{2}(\tilde{h}^i{}_k\tilde{h}^j{}_l - \tfrac{1}{2}\tilde{h}^{ij}\tilde{h}_{kl})\tilde{u}^{kl}|_{\mathcal{S}}, \quad (30)$$

where $\tilde{D}^i$ denotes the covariant derivative compatible with $\tilde{h}_{ij}$. Below, we will assume $\tilde{u}_{ij} = 0$; in that case, Eq. (30) implies that ${\beta_\parallel}^i$ must be a conformal Killing vector of the conformal metric, $\tilde{h}_{ij}$ on the boundary $\mathcal{S}$:

$$\tilde{D}^{(i}{\beta_\parallel}^{j)}|_{\mathcal{S}} - \tfrac{1}{2}\tilde{h}^{ij}\tilde{D}_k{\beta_\parallel}^k|_{\mathcal{S}} = 0. \quad (31)$$

In practice, we write the parallel components of the shift as

$${\beta_\parallel}^i = \Omega_r\xi^i, \quad (32)$$

where ξ^i is a rotational conformal Killing vector on $\tilde{h}_{ij}$ with affine length of 2π, and Ω_r is a constant. As shown in Ref. [5], the choice of ${\beta_\parallel}^i$ directly parametrizes the spin of the associated black hole. The restriction on ${\beta_\parallel}^i$ is quite remarkable. Regardless of the choice of the conformal metric $\tilde{\gamma}_{ij}$ (and thus for any $\tilde{h}_{ij}$), Eq. (31) still allows sufficient freedom to allow for the parametrization of a rotation about any direction (by the choice of ξ^i) and with any magnitude (by the choice of Ω_r) [5].

To summarize, the quasiequilibrium conditions defined in Eqs. (17), (18), and (22) define boundary conditions on the conformal factor, ψ, via Eq. (29) and on the shift vector, β^i, via Eqs. (26) and (32). These total to four of the five necessary boundary conditions for solving the coupled elliptic equations associated with the conformal thin-sandwich equations. Missing is a condition on the conformal lapse, $\tilde{\alpha}$.

However, as clearly shown in Ref. [5], the excision boundary condition on the lapse is intimately associated with a degeneracy in the choice of the initial slicing condition. In fact, for stationary black-hole spacetimes, it is the choice of the lapse on the excision boundary that uniquely fixes a particular initial slice. For initial data representing systems that are nearly stationary, that is systems in quasiequilibrium, it has also been shown that the choice of the excision boundary condition for the lapse is largely irrelevant. Following Ref. [5], we will choose the excision boundary condition for the lapse from a set of convenient and rather generic conditions. Assuming that the excision boundary is spherical, we use

$$\left.\frac{d\alpha\psi}{dr}\right|_{\mathcal{S}} = 0, \quad (33a)$$

$$\left.\frac{d\alpha\psi}{dr}\right|_{\mathcal{S}} = \left.\frac{\alpha\psi}{2r}\right|_{\mathcal{S}}, \quad (33b)$$

$$\alpha\psi|_{\mathcal{S}} = \tfrac{1}{2}. \quad (33c)$$

C. Quasicircular orbits

The formalism reviewed so far in Secs. II A and II B provides a very general framework for constructing initial data for black-hole binaries. Let us now make a specific choice for part of the freely specifiable initial data. Consider the choice $\tilde{u}_{ij} \equiv \partial_t\tilde{\gamma}_{ij} = 0$. This choice implies that the conformal three-geometry is, at least momentarily, stationary with respect to the time vector, $\mathbf{t}$, given by Eq. (21). Our choice for the boundary condition on the shift at infinity given in Eq. (16b) implies that our time vector has a *helical* form where the amount of "twist" in the vector is parametrized by $\Omega_0 \equiv |\mathbf{\Omega}_0|$.

If we assume that $\mathbf{t}$ is an approximate Killing vector of the spacetime, then $\tilde{u}_{ij} = 0$ is a direct consequence. With a proper choice of Ω_0, the resulting initial data represents a binary system where the black holes are in quasicircular orbits. This statement begs two questions: (1) How do we determine the proper choice of Ω_0 so as to obtain quasicircular orbits? (2) How do we interpret the initial data for other choices of Ω_0?

An answer to the first question was proposed by Gourgoulhon *et al.* [7] where they made the ansatz that Ω_0 be chosen so that the ADM mass [13] and the Komar mass [12] agree. We call this the "Komar-mass ansatz," and when it is applied, we refer to it as the "Komar-mass condition."

The ADM energy is an invariant definition of the total energy of a spacetime as measured by an inertial observer at spacelike infinity. The ADM energy is written as a surface integral at infinity

$$E_{\rm ADM} = \frac{1}{16\pi}\oint_\infty \nabla_j(\mathcal{G}^j_i - \delta^j_i\mathcal{G})d^2S^i, \quad (34)$$

where $\mathcal{G}_{ij} \equiv \gamma_{ij} - f_{ij}$, $\mathcal{G} = \gamma^{ij}\mathcal{G}_{ij}$, and f_{ij} is a flat metric. If the total linear momentum of the system (as measured by the same inertial observer at infinity) vanishes, then the ADM energy is usually referred to as the ADM mass. In our notation, the Komar mass can be written as

$$M_{\rm K} = \frac{1}{4\pi}\oint_\infty (\nabla_i\alpha - \beta^j K_{ij})d^2S^i. \quad (35)$$

The Komar mass is a valid expression for the total mass of a system only when the system possesses a global timelike Killing vector so that the system is stationary. It is therefore quite reasonable to assume that by choosing Ω_0 so that the Komar-mass ansatz will yield initial data which is nearly

stationary (i.e. in quasiequilibrium), which would require that the black holes be in quasicircular orbits.

The effectiveness of the Komar-mass ansatz has been tested numerically in black-hole initial data by comparison with post-Newtonian data for binaries in circular orbits [5,10] (and for neutron-star binaries [14]). There are also additional theoretical reasons for expecting that configurations satisfying the Komar-mass condition ($E_{\rm ADM} = M_{\rm K}$) will represent systems in quasiequilibrium (cf. Refs. [7,29] and references therein). These arguments show that a system in quasiequilibrium necessarily satisfies the Komar-mass ansatz. However, as far as we know, there is no guarantee that a system satisfying the Komar-mass condition is necessarily in quasiequilibrium. It would therefore be interesting to compare the Komar-mass ansatz against an independent method for determining circular orbits. The effective-potential method [9] will be used below to provide such a comparison.

It is worth noting that, when using the Komar-mass ansatz in the context of binary systems, care must be used in evaluating Eq. (35). An observer moving along the approximate helical Killing vector $\mathbf{t}$ is not an inertial observer. For a true stationary spacetime, the helical Killing vector can be split globally into separate timelike and rotational Killing vectors and the timelike Killing vector is used to define the timeline of the inertial observer making the measurements. The approximate helical Killing vector cannot be split globally, however it can be split *asymptotically* at spacelike infinity. In evaluating the Eq. (35), it is necessary to remove the $\mathbf{\Omega}_0 \times \mathbf{r}$ term from the shift, β^i so that the same inertial observer is used to evaluate both $M_{\rm K}$ and $E_{\rm ADM}$. Often, the Komar mass is written in a form similar to that of Eq. (35), but with the term involving the shift absent. In many cases, this yields a correct expression for the Komar mass since the contraction of the shift with the extrinsic curvature falls off faster than $1/r^2$ when the $\mathbf{\Omega}_0 \times \mathbf{r}$ contribution to the shift is omitted. However, it is *not* always correct to simply drop this term. For example, in Painlevé-Gullstrand coordinates [30–32] and their extension to the full Kerr-Newman spacetime [33], this term contains *the entire contribution to the Komar mass*.

In order to answer the second question of how to interpret the initial data when Ω_0 is no longer chosen via the Komar-mass condition, we must no longer think of the helical time vector as an approximate Killing vector of the spacetime. A more general interpretation of the choice $\tilde{u}_{ij} \equiv \partial_t \tilde{\gamma}_{ij} = 0$ is that the "velocity" of the conformal three-geometry vanishes on the initial-data slice. In the context of a binary configuration this suggests that the system is at either pericenter or apocenter of some general bound or unbound orbit. When $\Omega_0 = 0$, the system will have no orbital angular momentum and will represent a generalized version of Misner [34] or Lindquist [35,36] initial data.

D. Corotating and nonspinning black-hole binaries

In constructing black-hole binary initial data, we will certainly need the ability to specify the spins of the individual black holes. In Sec. II B, we mentioned that the excision boundary condition on the parallel components of the shift, ${\beta_\parallel}^i$, can be used to set the spin of each black hole. It is tempting to want to interpret Ω_r in Eq. (32) as the rotational angular velocity of the black hole. However, this is not the case. To understand the role of ${\beta_\parallel}^i$ in determining the spin on the black holes, it is useful to consider the special cases of corotating and nonspinning black holes. While neither case is expected to be seen astrophysically, these cases are useful because they represent situations where we know either what the boundary condition should be or what the final spin should be.

Corotating black-hole binaries represent the case where the black holes are rotating synchronously with the orbital motion. A great deal of attention has been paid to such binaries because they represent the only configuration of two black holes that can possess a *true* helical Killing field [29,37–41]. A serious fault with such spacetimes is that they cannot be asymptotically flat since they contain a balancing amount of incoming and outgoing radiation for all time. However, for our purposes, they are ideal. First, because we at most have only an approximate helical Killing vector, we can still have an asymptotically flat solution. More importantly, we know that the corotating case possesses a Killing horizon. This means that the proper choice for the parallel components of the shift is unambiguously given by ${\beta_\parallel}^i = 0$.

Since corotating black holes necessarily have some nonvanishing rotation (and therefore spin) as seen by an asymptotic inertial observer, clearly Ω_r cannot represent the rotational angular velocity of the black hole. At least for a Newtonian binary system in corotation, the rotational angular velocity should equal the orbital angular velocity of the binary system. For post-Newtonian computations of corotating black-hole binaries, this is, in fact, the condition used to set the spins of the black holes [10,42]. To leading order, this is correct. However, as we will demonstrate below, higher-order corrections are needed to correctly estimate the rotational angular velocity of corotating black holes.

Nonspinning black-hole binaries are, in some sense, the simplest case. Here, the individual black holes have no spin as measured by an asymptotic inertial observer. In previous works, we have referred to such systems as having "irrotational" black holes [5,6]. Perhaps, however, this is not the best terminology as it carries with it the notion of fluid motion which is not appropriate for black holes. From now on, we will refer to such black holes as being "nonspinning." How do we choose ${\beta_\parallel}^i$ to yield black holes with no spin? We argued previously [5] that, for a binary with orbital angular velocity Ω_0, we should choose $\Omega_r = \Omega_0$.

Also, for spherical excision boundaries, we chose ξ_i as the flat-space rotational Killing vector, projected into the excision surface, that generates a rotation about an axis parallel to the orbital angular momentum vector. We also showed that this condition led to reasonable results. To leading order this is correct, but again we will show below that it is necessary to modify this choice for the boundary condition in order to produce nonrotating black-hole binaries.

E. Conformally flat maximally sliced models

So far, we have discussed the approach used to construct binary initial data in rather general terms. We have discussed the conformal thin-sandwich decomposition and the choice of boundary conditions for constrained variables within that formalism. These constrained variables $(\psi, \beta^i, \tilde{\alpha})$ can only be determined after values for the unconstrained variables $(\tilde{\gamma}_{ij}, \tilde{u}_{ij}, K, \partial_t K)$ have been chosen. In Sec. II C, we discussed the interpretation of initial data when the choice $\partial_t \tilde{\gamma}_{ij} \equiv \tilde{u}_{ij} = 0$ was made. We will use this choice for $\tilde{u}_{ij}$ in all models constructed below.

We will also make the assumption of *conformal flatness* in all of the models we construct. That is, we will choose $\tilde{\gamma}_{ij}$ to be a flat metric. This choice impacts upon the physical content of the initial data that we will construct. It is well known that the spatial metric for a relativistic binary system cannot be conformally flat [43], nor can the spatial metric of a stationary spinning black hole [44,45] or even the metric of a boosted black hole. However, the errors introduced by the assumption of conformal flatness are not ''grave.'' There are efforts underway to improve the choice of the conformal metric. Some of these efforts involve using an analytic metric obtain from post-Newtonian theory (cf. Ref. [46]). However a more self-consistent approach has been developed by Shibata *et al.* [47,48] for the case of neutron-star binaries and it should be possible to adapt this approach to black-hole binaries in the future.

Finally, we choose to use maximal slicing, $K = \partial_t K = 0$, in all of the models we construct. Which member of the family of possible maximal slices we choose will depend upon our choice for the boundary condition for the lapse [5]. As a slicing condition, we do not expect this choice to impact significantly upon the physical content of the initial data.

F. Numerical code

We solve the elliptic equations of the conformal thin-sandwich decomposition using the pseudospectral collocation method described in Refs. [5,49]. As usual with spectral methods (see, e.g. [50]), the solution is expressed as a truncated series of basis functions, and is represented by a set of expansion coefficients. For appropriate basis functions, discretization errors decay exponentially with the number of retained basis functions [50]. The elliptic equations take the form of a set of nonlinear algebraic equations for the expansion coefficients. These algebraic equations are solved with a Newton-Raphson method, where in each step a linear problem is solved via standard Krylov subspace techniques [51] like preconditioned fGMRES [52].

For the binary black-hole solutions of this paper, we need to solve elliptic equations in a computational domain with two excised spheres. To do so, the computational domain is split into smaller subdomains, namely, spherical shells and rectangular blocks. A shell is placed around each excision surface and a third shell, using a compactified radial coordinate, extends from some intermediate radius surrounding both holes out to the outer boundary which is typically placed at a radius of $\sim 10^8$. The space between is filled by a collection of rectangular blocks.

Further details of the numerical code can be found in Ref. [5]. In particular, Fig. 6 of Ref. [5] displays the convergence of the code for a typical configuration. The calculations below were performed at a resolution comparable to $N = 60$ in this figure and correspond to discretization errors on the order of 10^{-5} or 10^{-6} for most of the quantities we consider.

III. COMPUTING THE QUASILOCAL SPIN OF A BLACK HOLE

In the previous discussion, we referred to the spin of an individual black hole in a binary system. However, there is no unique, rigorous definition of the spin of a black hole unless it is in isolation and stationary. We can, however, rigorously define the total angular momentum of an initial-data slice as measured by an inertial observer at infinity. Usually referred to as the ADM angular momentum, it can be expressed as

$$J_{(\xi)} = \frac{1}{8\pi} \oint_\infty (K_{ij} - \gamma_{ij} K) \xi^j d^2 S^i, \tag{36}$$

where ξ^i is a Killing vector of γ_{ij}. For asymptotically flat data, we can choose this to be each of the three flat-space rotational Killing vectors in order to determine the three components of the total angular momentum of the system.

Although there is no unique, rigorous definition for the spin of an individual black hole in general, we can estimate the spin based upon a quasilocal definition. There are many different quasilocal definitions for spin [15]. While motivated in different ways, they tend to take on a similar form within a 3 + 1 framework. One of the earliest useful definitions was derived by Brown and York [16]. This same definition was rederived more recently within the *isolated* and *dynamical horizons* framework of Ashtekar and Krishnan [17,18]. In either case, the quasilocal spin can be expressed as

$$S_{(\xi)} = \frac{1}{8\pi} \oint_S (K_{ij} - \gamma_{ij} K) \xi^j d^2 S^i, \tag{37}$$

where now ξ^i is a Killing vector of h_{ij}. We note the remarkable similarity between Eqs. (36) and (37). The main difference between them is that the former is evaluated at infinity while the latter is evaluated on the apparent horizon. For the initial data we are constructing, this will be the excision surface. In terms of the variables used in the conformal thin-sandwich decomposition, we evaluate the spin as

$$S_{(\xi)} = \frac{1}{16\pi} \oint_{\mathcal{S}} \frac{1}{\tilde{\alpha}} [(\tilde{\mathbb{L}}\beta)_{ij} - \tilde{u}_{ij}] \xi^j \tilde{s}^i \sqrt{\tilde{h}} d^2x, \tag{38}$$

where we have used the fact that ξ^i is tangent to the excision surface, i.e. $\tilde{\gamma}_{ij}\xi^i\tilde{s}^j = 0$.

The only choice that must be made in evaluating the spin is to choose the Killing vector ξ^i. The problem is that, in general, an exact Killing vector will not exist. However, there are two reasonable choices that can be made. If our excision surface (apparent horizon) is a coordinate sphere within our flat conformal geometry, then we can choose to approximate ξ^i by one of the 3 flat-space rotational Killing vectors centered on the excision sphere and projected onto its surface. We will denote these three choices by

$$\xi^i_{(x)} = x^j_s \epsilon^{ixj}, \tag{39a}$$

$$\xi^i_{(y)} = x^j_s \epsilon^{iyj}, \tag{39b}$$

$$\xi^i_{(z)} = x^j_s \epsilon^{izj}, \tag{39c}$$

where we assume Cartesian coordinates and $\mathbf{x}_s$ is measured relative to the center of the excision sphere.

An alternative is to attempt to solve Killing's equation. Once we have solved the constraint equations and have full initial data, we know h_{ij}, the physical metric projected onto the excision surface $\mathcal{S}$. In Ref. [27], Dreyer *et al.* outlined a general method for finding the Killing vectors on a closed 2-surface. We give the details of our implementation of this method in Appendix A. Here, we simply note that exact solutions of Killing's equation will not exist in general so what we find are "approximate" Killing vectors.

It is difficult to make a meaningful quantitative measure of how far a given solution deviates from being a true Killing vector. For our purposes, we will attempt to gauge the accuracy of our measured spins by comparison with expected values. For the case of corotating black holes, we know that our boundary condition on ${\beta_{\|}}^i$ is correct and we know, at least to leading order, what the spin of a corotating black hole should be in a binary. Thus, we can compare our quasilocal definition for the spin of a black hole against an analytic result.

Below, when we discuss the computed quasilocal spin, we will use the following notation for simplicity:

$$\begin{aligned} &S_x\text{: computed using Eq. (39a)} \\ &S_y\text{: computed using Eq. (39b)} \\ &S_z\text{: computed using Eq. (39c)} \\ &S_K\text{: } \begin{cases} \text{computed using an approximate} \\ \text{solution of Killing's equation.} \end{cases} \end{aligned} \tag{40}$$

IV. COROTATING BINARIES

Although corotation is not considered to be an astrophysically realistic state for black-hole binaries, it is an important test case because it is the one configuration for black-hole binaries that is compatible with a true helical Killing vector [29,37,38]. The thermodynamic relations obtained by Friedman *et al.* [29],

$$\delta E_{\mathrm{ADM}} = \Omega_0 \delta J_{\mathrm{ADM}} + \sum \kappa_i \delta \mathcal{A}_i, \tag{41}$$

should apply to our conformally flat data if we had a true helical Killing vector and we assume no local change in entropy. In Eq. (41), J_{ADM} is the magnitude of the total ADM angular momentum of the system, κ_i and $\mathcal{A}_i$ are, respectively, the surface gravity and area of the Killing horizon of each black hole. Corotating black holes also have a nonvanishing spin and, more importantly, a physically well-defined notion of the rate of rotation. Together, these give us a firm analytic foundation against which we can test our initial data.

Let us first consider the thermodynamic identity in Eq. (41). We are free to define a fundamental length scale for each of our initial-data solutions. We can use this freedom to scale our solutions in an attempt to have it satisfy this identity. Of course, Eq. (41) allows for too much variation for a single length rescaling to guarantee the enforcement of the identity in general. However, we can use the freedom to define a fundamental length scale $\chi(s)$ along a sequence of initial data to enforce

$$\delta E_{\mathrm{ADM}} = \Omega_0 \delta J_{\mathrm{ADM}}. \tag{42}$$

This approach has been discussed previously [5,8], but for completeness, we cover it again here.

Using our freedom to define the fundamental length scale $\chi(s)$ along a sequence we define the dimensionful total energy $E_{\mathrm{ADM}}(s)$, total angular momentum $J_{\mathrm{ADM}}(s)$, and orbital angular velocity $\Omega_0(s)$ consistently via

$$E_{\mathrm{ADM}}(s) \equiv \chi(s) e(s), \tag{43}$$

$$J_{\mathrm{ADM}}(s) \equiv \chi^2(s) j(s), \tag{44}$$

$$\Omega_0(s) \equiv \chi^{-1}(s) \omega(s). \tag{45}$$

Then, to enforce Eq. (42), it is sufficient to determine the change in $\chi(s)$ between two points on the sequence. This can be done by integrating along the sequence from a point

TABLE I. The irreducible mass $M_{\rm irr}$ of a single black hole in a corotating, nonspinning, and leading-order (LO) nonspinning binary as we vary the coordinate separation d. The length scale is set so that the ADM mass of the binary at very large separation is 1. Lapse boundary condition (33b) was used for all data.

	$M_{\rm irr}$		
d	Corotation	Nonspinning	"LO" nonspinning
40	0.500 000 0	0.500 000 0	0.500 000 0
35	0.500 000 1	0.500 000 1	0.499 998 8
30	0.500 000 2	0.500 000 2	0.499 996 6
25	0.500 000 5	0.500 000 5	0.499 990 2
20	0.500 001 0	0.500 001 1	0.499 972 7
19	0.500 001 3	0.500 001 4	0.499 965 9
18	0.500 001 6	0.500 001 7	0.499 956 8
17	0.500 002 0	0.500 002 1	0.499 944 6
16	0.500 002 5	0.500 002 6	0.499 928 1
15	0.500 003 2	0.500 003 3	0.499 905 0
14.5	0.500 003 7	0.500 003 7	0.499 890 1
14	0.500 004 2	0.500 004 2	0.499 872 1
13.5	0.500 004 8	0.500 004 8	0.499 850 4
13	0.500 005 6	0.500 005 5	0.499 823 8
12.5	0.500 006 5	0.500 006 4	0.499 791 1
12	0.500 007 6	0.500 007 4	0.499 750 4
11.5	0.500 009 0	0.500 008 6	0.499 699 2
11	0.500 010 7	0.500 010 2	0.499 634 0
10.5	0.500 012 9	0.500 012 0	0.499 549 8
10	0.500 015 7	0.500 014 4	0.499 439 3
9.5	0.500 019 3	0.500 017 3	0.499 291 8
9	0.500 024 0	0.500 021 1	0.499 090 8
8.5	0.500 030 8	0.500 025 9	0.498 809 1
8	0.500 040 1	0.500 033 0	0.498 400 8
7.5	0.500 052 9	0.500 042 3	0.497 781 5
7	0.500 070 2	0.500 054 6	0.496 784 2

s_1 to another point s_2. Doing so, we find[1]

$$\chi(s_2) = \chi(s_1) \exp\left\{ - \int_{s_1}^{s_2} \frac{e'(s) - \omega(s) j'(s)}{e(s) - 2\omega(s) j(s)} ds \right\}, \quad (46)$$

where a prime denotes differentiation along the sequence.

Now, if the Komar-mass ansatz is reasonable, then a sequence of initial data with varying separation that satisfies this ansatz should represent a binary in a nearly adiabatic evolutionary sequence of quasicircular orbits that satisfy Eq. (41). But, having scaled the data to satisfy Eq. (42), the identity in Eq. (41) has been reduced to $\sum \kappa_i \delta \mathcal{A}_i = 0$. To leading order, $\kappa = 1/4M_{\rm irr}$ for each hole. Together with the definition of the irreducible mass

$$M_{\rm irr} = \sqrt{\frac{A_{\rm AH}}{16\pi}}, \quad (47)$$

where $A_{\rm AH}$ is the area of the black hole's apparent horizon, we find $\kappa \delta \mathcal{A} \approx 8\pi \delta M_{\rm irr}$ for each black hole. So, if the Komar-mass ansatz is reasonable we should find that $\sum (\delta M_{\rm irr})_i \approx 0$ along a sequence of initial-data sets.

The second column of Table I lists the irreducible mass of one corotating black hole as we vary the orbital separation and enforce Eq. (42). Given our excision boundary condition, Eq. (26), the apparent horizon is, at least instantaneously, a Killing horizon. The only deviation we should expect in $M_{\rm irr}$ should be due to the fact that we do not have a true helical Killing vector and that the apparent horizon is not part of a global Killing horizon. As we see from the table, $M_{\rm irr}$ changes only by about one part in 10^4 over the entire sequence of separations. While small, the variations seen in $M_{\rm irr}$ are larger than the level of accuracy of the initial-data computations and the leading digits of the variation are also above the level of truncation error that result from integrating Eq. (46). Thus, the variation in $M_{\rm irr}$ seems to be a true artifact of our approximate helical symmetry. On the other hand, it is quite small and this lends support to the Komar-mass ansatz.

A. Effective-potential method

Another way of testing the Komar-mass ansatz is to use an independent method for identifying circular orbits. An "effective-potential" method for determining circular orbits from sequences of initial-data sets was outlined in Ref. [9]. This method is motivated by variational techniques, but does not have a rigorous theoretical foundation. Nevertheless, it has been used successfully for black-hole binary initial data [9,53,54] and has been shown to agree with the Komar-mass condition in the case of circular orbits for thin shells of collisionless matter [55]. Agreement between the two methods was also demonstrated, within error bars, at the location of the innermost stable circular orbit of sequences of circular orbits produced using puncture data [56] (which uses different and more simplifying assumptions).

The method is straightforward, but has one significant point of ambiguity. The effective-potential (EP) method identifies circular orbits as configurations with a minima in the binding energy along sequences of configurations where the total angular momentum is held fixed. The ambiguity is associated with the same freedom to define the fundamental length scale mentioned above. In Ref. [9], this ambiguity was resolved by demanding that the mass of each black hole as defined by the Christodoulou formula [57] be held constant along sequences of configurations.

The Christodoulou formula

$$M^2 = M_{\rm irr}^2 + \frac{S^2}{4M_{\rm irr}^2} \quad (48)$$

includes the spin of the black hole which adds another level of complication. The EP method was originally applied only to configurations in which the direction and magnitude of the spin was also held constant along sequences

[1]Note that the similar equation in Ref. [5] contains a factor of 2 error in the denominator of the integrand.

of configurations. With this restriction, holding the Christodoulou mass M constant was equivalent to holding the irreducible mass $M_{\rm irr}$ constant. Furthermore, with this restriction on the spin, finding minima of the binding energy was equivalent to finding minima of the ADM energy.

However, when we consider sequences of corotating binaries, the magnitude of the spins of the black holes are no longer held constant and we must reconsider how we will fix the mass freedom. From Friedman *et al.* [29] and the results shown above, is seems clear that we should hold the irreducible mass (or the area of the apparent horizon) fixed along sequences of configurations. We will define the total mass m and reduced mass μ as

$$m \equiv M_{\rm irr1} + M_{\rm irr2}, \tag{49}$$

$$\mu \equiv \frac{M_{\rm irr1} M_{\rm irr2}}{m}, \tag{50}$$

and then the binding energy E_b by

$$E_b \equiv E_{\rm ADM} - m. \tag{51}$$

With this definition of the binding energy, minima of the binding energy and the ADM energy agree for corotating configurations as well as for sequences with the spins held fixed (so long as we also hold the individual irreducible masses fixed).

We will, therefore, adopt the following functional definition for the EP method. We will take as configurations with circular orbits those initial data configurations that have a minimum of the ADM (or binding) energy along sequences of configurations where the total angular momentum, irreducible masses of the black holes, and direction of the black holes spins are held fixed. This definition is sufficient to handle both corotating and nonrotating black-hole binaries. The case of black holes with arbitrary spin will be considered in future investigations.

Figure 1 is a plot of the dimensionless binding energy E_b/μ as a function of the dimensionless proper separation ℓ/m between the apparent horizons for equal-mass corotating black holes. Each line of constant total angular momentum $J/\mu m$ is an "EP curve" and the local minimum of that curve represents the circular-orbit configuration having that value of the total angular momentum. Passing through the set of minima, and plotted with a solid line, is the EP sequence of circular orbits. At small separations, this sequence terminates at the inflection point on the first EP curve that does not contain a local minimum. This is the short EP curve having $J/\mu m \approx 3.38$. The inflection point in the EP curves marks the termination of stable circular orbits and the configuration at the point is referred to as the "innermost stable circular-orbit" (ISCO) configuration. Also plotted in this figure with a dashed line is the sequence of circular orbits as defined by the Komar-mass ansatz. For a Komar sequence, the ISCO configuration is defined as the model with the minimum binding energy. Notice that the Komar and EP sequences are nearly coincident except for the regime near the ISCO.

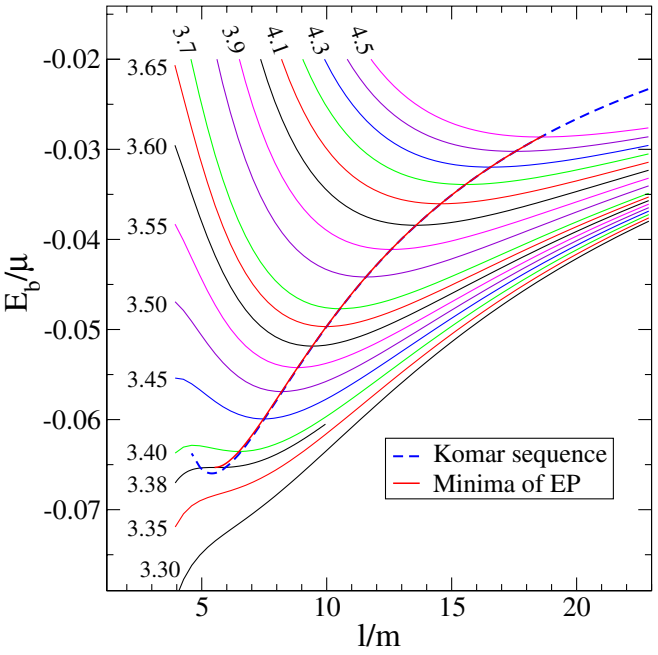

FIG. 1 (color online). Effective-potential (EP) curves E_b/μ for corotating black holes vs separation ℓ/m. These curves are labeled by the orbital angular momentum $J/\mu m$ which is kept constant along each curve. The thick red line connecting the minima of the EP curves represents circular orbits; it terminates at the innermost stable circular orbit at the inflection point in the EP curve at $J/\mu m = 3.38$. Also plotted as a dashed blue line is the sequence of circular orbits determined by the Komar-mass ansatz.

A more quantitative comparison of the sequences obtained via the Komar-mass ansatz and the EP method is found by examining the error in the Komar-mass condition for circular orbits along a sequence of such orbits defined by the EP method. Figure 2 plots this error, $M_{\rm K} - E_{\rm ADM}$, scaled relative to the ADM energy versus the 5/2-power of the dimensionless orbital angular velocity $m\Omega_0$. Interestingly, we see that the relative error is nearly linear in $(m\Omega_0)^{5/2}$. We see that the deviation is quite small, even at the ISCO near $(m\Omega_0)^{5/2} \sim 0.0032$, where the error is roughly 0.015%. From the jaggedness of the curve at large separations (small $m\Omega_0$), it is evident that the errors are nearing the level of truncation error for the measurement of the energies. However, the measured deviation is clearly physical, not numerical.

We see that the Komar-mass condition and the EP method appear to agree to a very high degree in determining configurations with circular orbits. But, there is a measurable difference. As a final comparison, we can rescale the sequence of circular orbits defined by the EP method so as to satisfy Eq. (42) just as was done for the sequence defined by the Komar-mass condition. When we

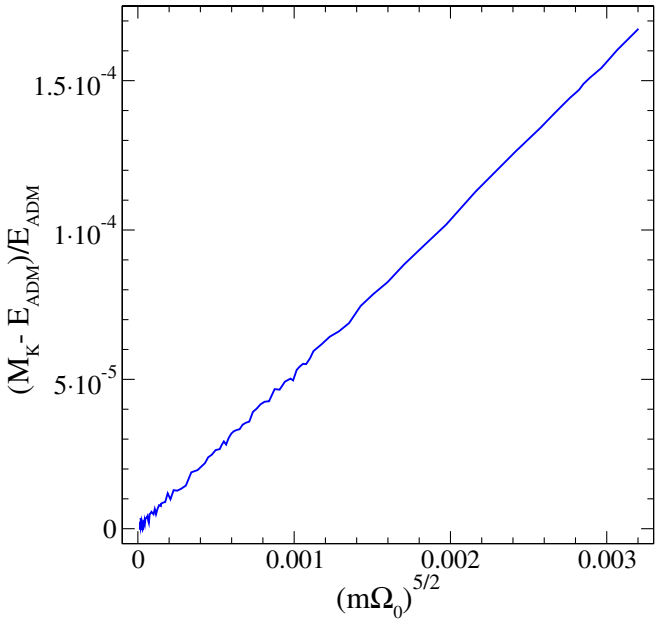

FIG. 2 (color online). Violation of the Komar-mass condition when the effective-potential method is used to determine the sequence of circular orbits. Here, corotating equal-mass binaries are considered. $m\Omega_0$ denotes the orbital angular frequency, so that large separations correspond to small values of $m\Omega_0$.

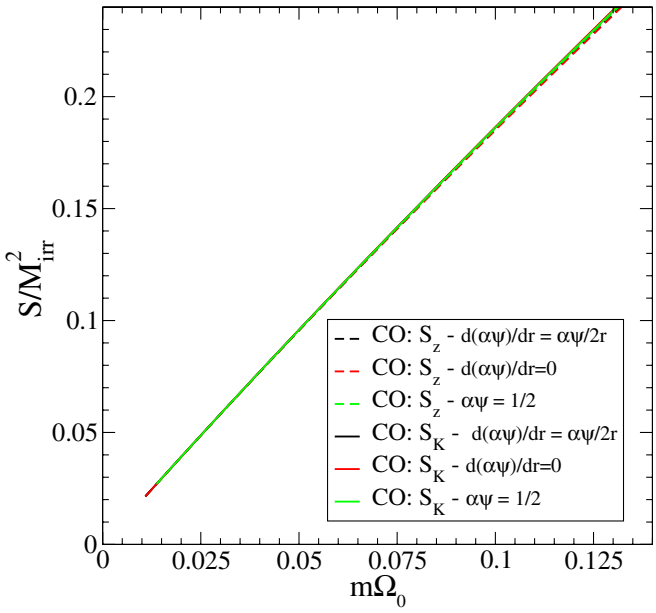

FIG. 3 (color online). Quasilocal spin $S/M_{\rm irr}^2$ of a black hole in a corotating equal-mass (CO) binary along the sequence of circular orbits (parametrized by the orbital angular velocity $m\Omega_0$). S_z and S_K are defined in Eq. (40). Results are given for sequences with three different lapse boundary conditions.

examine the variation of $M_{\rm irr}$ along the rescaled EP sequence, we find the largest deviations are more than a factor of 100 smaller than those seen in the sequences defined by the Komar-mass condition displayed in Table I. This level of variability is consistent with the level of truncation error in the numerics. Thus, to the numerical precision of the calculations, we find that the sequence of corotating equal-mass binaries in circular orbits defined by the EP method satisfies the thermodynamic identity of Eq. (41).

B. Spin

Another reason for considering corotating binaries is that we want to calibrate our techniques for computing the quasilocal spin of a black hole, and corotating binaries have a physically well-defined notion of the rate of rotation of each black hole. From a Newtonian perspective, a corotating binary has the rotational angular velocities of the individual objects equal to the orbital angular velocity. But, this is a nonlocal statement and, as such, is not well defined in the context of general relativity. A relativistically reasonable notion of corotation might be to connect the rate of rotation of one black hole with the local rate of rotation of tidal perturbations due to the orbit of its companion.

We begin by first computing the spin of each black hole as a function of the orbital angular velocity Ω_0 along a sequence of circular orbits that satisfy the Komar-mass condition. In Fig. 3, we plot the quasilocal spin as computed by Eq. (38) for the three lapse boundary conditions listed in Eqs. (33) and for the cases where ξ^i is defined via the flat-space Killing vectors or via an approximate Killing vector as described in Sec. III. When computed using the flat-space Killing vectors as define by Eqs. (39), we note that S_x and S_y vanish to roundoff error. We see that all cases show very close agreement for the spin of the black holes. Also, recall that we expect our results to be largely independent of the choice of the lapse boundary conditions and plot the results from different lapse boundary conditions to confirm this conjecture.

While the various measures of the spin agree well, we have yet to determine if the magnitude of the spin is correct. To do so, we first note that the spin of a Kerr black hole, $S_{\rm Kerr}$, is given in terms of its irreducible mass $M_{\rm irr}$ and the rotational angular frequency of its horizon, Ω_B, by

$$S_{\rm Kerr}(M_{\rm irr}, \Omega_B) = \frac{4M_{\rm irr}^3\Omega_B}{\sqrt{1-4(M_{\rm irr}\Omega_B)^2}}. \qquad (52)$$

So, if we know the rotational angular frequency of the black hole's horizon, then we can check how well S_z and S_K satisfy Eq. (52). Conversely, by inverting Eq. (52) we can estimate the angular velocity Ω_B of the black hole in our numerical initial data from the measured quasilocal spins. It will be convenient to express this as

$$\frac{\Omega_B}{\Omega_0} = \frac{m}{M_{\rm irr}}\frac{1}{m\Omega_0}\frac{S/M_{\rm irr}^2}{4\sqrt{1+\frac{1}{4}(S/M_{\rm irr}^2)^2}}. \qquad (53)$$

In Ref. [5], we assumed that the rotational angular velocity of the black holes in a corotating binary was equal

to the orbital angular velocity $\Omega_B = \Omega_0$. We will refer to this assumption as the "leading-order" estimate. The lower six lines of Fig. 4 display the relative error between the measured quasilocal spin and the spin of a Kerr black hole, Eq. (52), with the same irreducible mass and with $\Omega_B = \Omega_0$. We see that the quasilocal spin estimate derived from the approximate Killing vectors is slightly better than the estimates based on the flat-space Killing vectors. Furthermore, the variation due to the lapse boundary condition is smaller for the approximate Killing vector cases. In all cases, the relative error is smaller than about 8% up to the ISCO which occurs near $m\Omega_0 \approx 0.1$, a quite large disagreement.

In order to make a better estimate of the error in the quasilocal spin measurements, we need a better estimate of the correct spin value. To improve on this estimate we note that Alvi [58] has computed the leading-order correction to the rotation rate Ω_T of the tidal field of a companion star as measured in the local asymptotic rest frame (LARF) [59] of a black hole

$$\Omega_T = \Omega_0\left[1 - \eta\frac{m}{b} + \mathcal{O}\left(\frac{m}{b}\right)^{3/2}\right], \tag{54}$$

where $\eta \equiv \mu/m$ and b is the separation of the black holes in harmonic coordinates. We can express this in a gauge independent way using a post-Newtonian expansion for b/m obtained for circular orbits [60]

$$\frac{m}{b} = (m\Omega_0)^{2/3}\left[1 + \left(1 - \frac{1}{3}\eta\right)(m\Omega_0)^{2/3} + \mathcal{O}(m\Omega_0)\right]. \tag{55}$$

Substituting, we find

$$\frac{\Omega_T}{\Omega_0} = 1 - \eta(m\Omega_0)^{2/3} + \Lambda(m\Omega_0) - \left[\eta\left(1 - \frac{1}{3}\eta\right) - \Gamma\right] \times (m\Omega_0)^{4/3} + \mathcal{O}(m\Omega_0)^{5/3}, \tag{56}$$

where Λ and Γ are functions of η coming from the unknown terms of order $(m/b)^{3/2}$ and $(m/b)^2$, respectively, in Eq. (54). The leading-order error term in Eq. (55), which includes spin-orbit coupling terms, contributes to the term of order $(m\Omega_0)^2$ in Eq. (56). We now make the physical assumption that Ω_T represents the angular velocity Ω_B at which a black hole should rotate in its LARF in order to be in corotation. This assumption improves the agreement with the Kerr-formula dramatically, as shown by the upper set of six lines in Fig. 4.

Figure 5 shows, from a different perspective, the improvement obtained by using Alvi's result. From Eq. (53), we obtain the expected value of Ω_B/Ω_0 from the initial data, *assuming* the Kerr formula is exactly satisfied. In Fig. 5, we show this expected value for Ω_B/Ω_0 for each of the three lapse boundary conditions and compare these to Ω_T/Ω_0 from Eq. (56). The dotted line labeled 1PN includes only the leading-order correction to Ω_T/Ω_0.

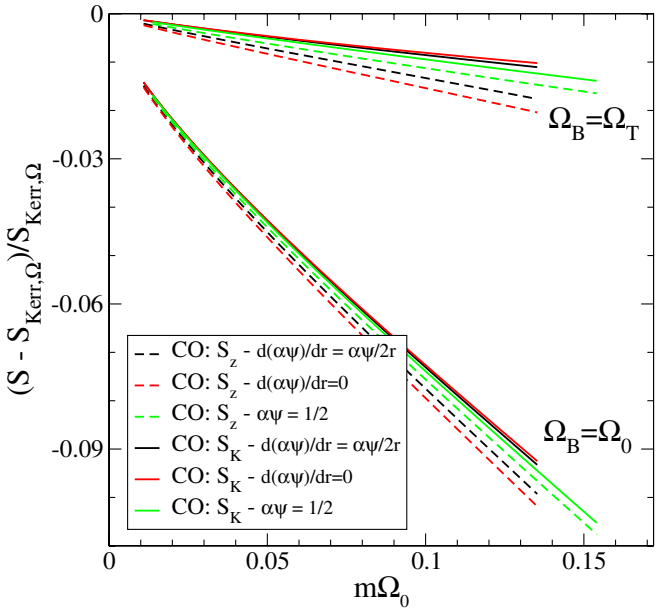

FIG. 4 (color online). Difference between the quasilocal spin of a black hole in a corotating (CO) binary and the result of the Kerr-formula Eq. (52). For the lower set of six lines ($\Omega_B = \Omega_0$), the rotation rate of the black hole is simply taken to be equal to the orbital angular velocity. For the upper set of six lines ($\Omega_B = \Omega_T$), the rotation rate is taken to be equal to that of the tidal field of the companion hole as measured in the LARF. Each set of six lines corresponds to the cases plotted in Fig. 3.

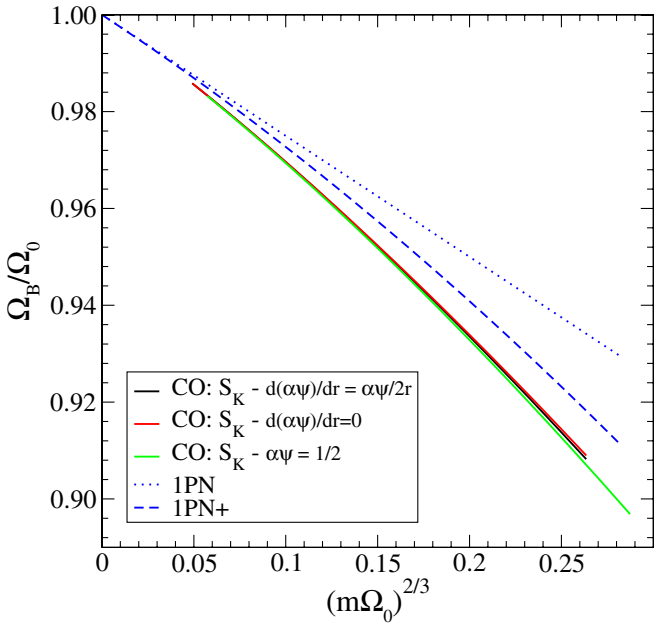

FIG. 5 (color online). Ratio of the rotational angular velocity Ω_B of a black hole, as determined from the quasilocal spin S_K, to the orbital angular velocity of the binary along the corotating (CO) sequence. The dotted line (labeled 1PN) represents the leading-order correction to the analytic estimate of the ratio. The dashed line (labeled 1PN +) shows the higher-order correction of Eq. (56) with $\Lambda = \Gamma = 0$. Numerical results are given for three different lapse boundary conditions.

Since we are plotting the ratio against $(m\Omega_0)^{2/3}$, this line is linear. The dashed line labeled 1PN+ shows the full analytic estimate assuming the unknown coefficients $\Lambda = \Gamma = 0$. For our equal-mass binaries, $\eta = 1/4$.

We see that the analytic estimate for the rotation rate is in reasonably good agreement with the numerical results. In fact, the difference between them is nearly linear in $m\Omega_0$ and is well fit by setting $\Lambda \sim -0.085$ (for the equal-mass case of $\eta = 1/4$ and $\Gamma = 0$). It would be quite interesting to determine the next term in the rate of rotation of the tidal field given in Eq. (54) since this term would fix Λ. We should note, however, that we cannot expect our estimates of the spin to agree perfectly with the higher-order analytic estimates of the black-hole rotation rate for corotation. There are two reasons for this. One is that our initial data is conformally flat. In Ref. [5], we examined the case of a single rotating, conformally flat black hole. Maximum rotation in a corotating binary occurs at ISCO where the rotational angular velocity has a value of $M_{\rm irr}\Omega_B \sim 0.05$. At this rate of spin, we expect the approximation of conformal flatness to introduce an error of about 0.02%. The second source of error is the quasilocal estimate of the spin itself which has some *a priori* unknown level of uncertainty. We show a rough indication of the current level of uncertainty in Fig. 4. In the top six lines, we again plot the relative error of the quasilocal spins, but now plotting the error relative to the Kerr spin based on the tidal rotation rate given by Eq. (56) with $\Lambda = \Gamma = 0$.

We see that at ISCO ($m\Omega_0 \sim 0.1$), the relative errors for the spins computed using an approximate Killing vector are all less than 1%, but significantly larger than the 0.02% error caused by the assumption of conformal flatness. Unfortunately, we cannot determine whether this remaining error is due to the inherent uncertainty of our quasilocal measure of the spin or to the unknown value of Λ (and higher-order terms). The only thing that we can conclude is that the uncertainty in the spin based on comparing the two different approaches to compute the spin is of the order of 1%, and is about 0.5% based on the uncertainty introduced by the different lapse boundary conditions. Both are of the same order as the total error which is remarkably small and gives us considerable confidence in our quasilocal spin measure.

V. NONSPINNING BINARIES

In order to model nonspinning binaries, we must choose an appropriate nonvanishing excision boundary condition on ${\beta_\parallel}^i$. Since our models are set up so that the orbital angular momentum is pointed in the positive z direction, we choose the boundary condition on ${\beta_\parallel}^i$ via Eq. (32) and set $\xi^i = \xi^i_{(z)}$, the flat-space Killing vector of Eq. (39c). This choice for ξ^i is appropriate because we have a spherical excision surface in a flat conformal geometry, so $\xi^i_{(z)}$ is a conformal Killing vector of the physical induced metric on the excision surface. The only freedom remaining in the boundary condition is the magnitude of Ω_r.

A. Leading-order approximation: $\Omega_r = \Omega_0$

In Ref. [5], it was argued that, at least to leading order, the correct choice for nonspinning black holes was to choose Ω_r to be equal to the orbital angular velocity, $\Omega_r = \Omega_0$. The numerical results were in good agreement with post-Newtonian estimates for sequences of equal-mass nonspinning binaries in circular orbits and with post-Newtonian estimates for the location of the ISCO. In this section, we revisit this argument with the new diagnostic tools presented earlier in this paper, in particular, effective potential plots and quasilocal measures of the spin.

Figure 6 displays several EP curves for the leading-order (i.e. $\Omega_r = \Omega_0$) nonspinning binaries where the total angular momentum is held fixed. It is immediately clear that the sequence of circular orbits determined by the Komar-mass condition does not intersect the minima of the EP curves. Furthermore, there does not appear to be an inflection point in the EP curves anywhere near the minimum of the Komar sequence of circular orbits. This clearly indicates that a problem of some kind exists.

The source of the problem is made clear by examining the quasilocal spins of black holes in our leading-order nonspinning models. The inset of Fig. 7 shows the magnitude of the spin on one of the black holes in the leading-

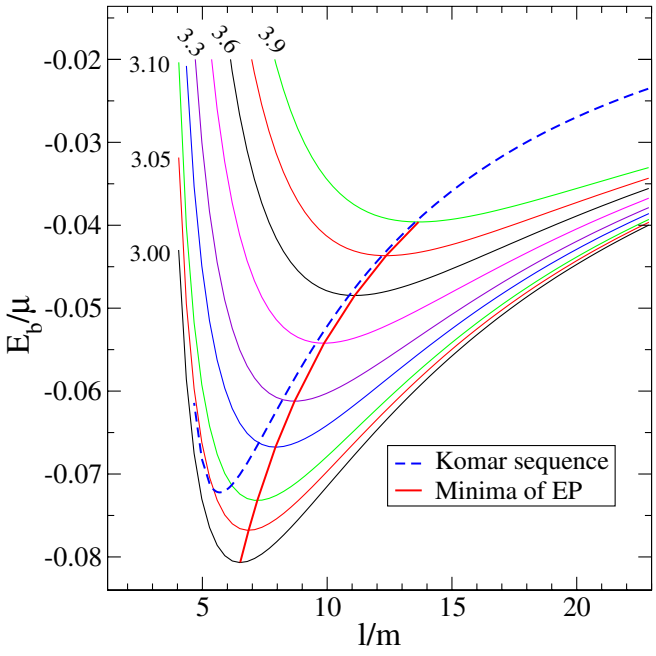

FIG. 6 (color online). EP curves E_b/μ for equal-mass "leading-order" nonspinning binaries ($\Omega_r = \Omega_0$) plotted vs separation ℓ/m. These curves are labeled by the value of $J/\mu m$ along each curve. Also plotted are the line connecting the minima of the EP curves, as well as the sequence of circular orbits as determined by the Komar-mass ansatz. The Komar-mass ansatz and the effective-potential method clearly disagree.

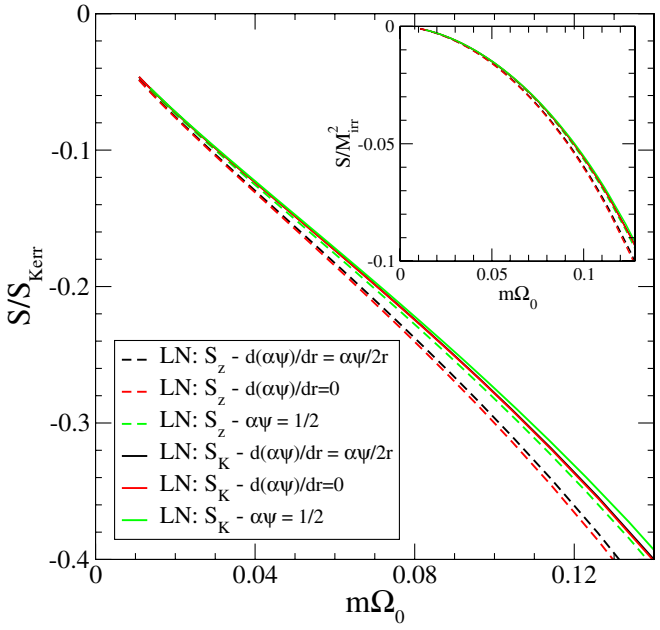

FIG. 7 (color online). Quasilocal spin of the "leading-order" nonspinning (LN) binaries (as shown in Fig. 6) plotted vs orbital angular velocity. The inset displays the dimensionless spin value $S/M_{\rm irr}^2$. The main figure displays the magnitude of the spin relative to the spin of a Kerr black hole with $\Omega_B = \Omega_0$. The residual spin is quite large.

order nonspinning equal-mass binary as a function of the orbital angular velocity. As in the corotating case, the x and y components of the spin vanish to roundoff error and we see that the z component of the spin computed using flat-space Killing vectors agrees well with the magnitude of the spin computed using an approximate Killing vector. But, it is clear that the magnitude of the spin is not zero. To get a better understanding of whether or not this magnitude of spin is small, Fig. 7 also compares this spin with the spin of a Kerr black hole having a rotational angular velocity equal to the binary's orbital angular velocity. Essentially, this is a measure of the magnitude of the spin relative to the corresponding corotating case.

We see that the spin for the leading-order nonspinning equal-mass binaries can be as large as 30% of the corotation spin at ISCO. This is clearly a significant deviation from the desired nonspinning configuration we wish to model.

Another indication that there is an error in the leading-order nonspinning equal-mass binaries is found in examining how well the sequence of leading-order nonspinning circular orbits agrees with the thermodynamic identity of Eq. (41). In Table I, we show the results for sequences of circular orbits constructed using the Komar-mass condition. The last column shows the results for leading-order nonspinning binaries. We find the disturbing result that the irreducible mass decreases as the binary evolves to smaller radii. More importantly, comparing this variation to that seen in the second column, we find that the size of the variation in $M_{\rm irr}$ for the leading-order nonspinning case is roughly 20 times larger than that seen in the corotating case (see also Fig. 9 of Ref. [5]). Of course, the thermodynamic identity was derived for corotating binaries, not nonspinning binaries, so we should not be surprised that it is not satisfied in this case, and by itself this failure is not too worrisome. However, the combined evidence in this section, in particular Figs. 6 and 7, makes it clear that the leading-order approximation $\Omega_r = \Omega_0$ is not satisfactory. Since we can now evaluate the quasilocal spin, we no longer have to choose Ω_r by some *ad hoc* prescription—instead, we can simply choose it such that the quasilocal spin vanishes. This approach will be explored in the following section.

B. Correct approach for nonspinning binaries

To correctly model nonspinning black-hole binaries, we need to choose Ω_r so that the quasilocal measure of the spin vanishes, $S_K = 0$. This will involve root finding, i.e., the constraints will have to be solved for different values Ω_r until the solution satisfies $S_K = 0$. Since the correct value of Ω_r for nonspinning black holes will be close to Ω_0, we define a rotation fraction f_r as

$$\Omega_r = f_r \Omega_0. \tag{57}$$

While the definition of f_r mirrors Eq. (56) from our comparison with post-Newtonian results, we note that those post-Newtonian results do *not* enter the construction of nonspinning binary black-hole initial data. In practice, we determine f_r so that the quasilocal spin based on the approximate Killing vector vanishes to about one part in 10^8 or better.

In Fig. 8 we first plot the EP curves for "true" nonspinning equal-mass black-hole binaries. The solid line passing through the minima of the EP curves is the sequence of circular orbits as defined by the EP method. This sequence terminates at small ℓ/m at the ISCO which is defined by the occurrence of an inflection point in an EP curve. Finally, plotted as a dashed line in this figure is the sequence of circular orbits as defined by the Komar-mass condition. It is immediately apparent that the EP curves have the correct qualitative behavior and that the Komar sequence of circular orbits, drawn as a dashed line, passes very close to the minima of the EP curves everywhere except near the ISCO.

In Fig. 9, we plot the value of the quasilocal spin of one black hole in an equal-mass binary as a function of the orbital angular velocity. The sequences are circular orbits defined by the Komar-mass condition and we include plots of the three different lapse boundary conditions for both definitions of the spin. By construction, the quasilocal spin defined by the approximate Killing vector is zero, $S_K = 0$. However, the quasilocal spin defined by the flat-space Killing vector (S_z) is not necessarily zero and is a rough measure of the uncertainty in our definition of the spin. For

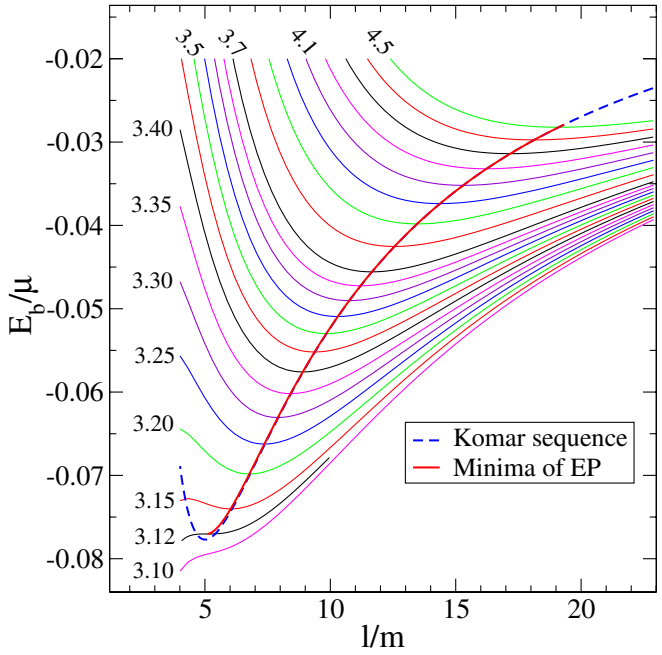

FIG. 8 (color online). EP curves E_b/μ for true nonspinning black holes vs separation ℓ/m. The curves are labeled by the orbital angular momentum $J/\mu m$ which is kept constant along each curve. The thick red line connecting the minima of the EP curves represents circular orbits, and terminates at the innermost stable circular orbit at the inflection point in the EP curve at $J/\mu m = 3.12$. Also plotted as a dashed blue line is the sequence of circular orbits as determined by the Komar-mass ansatz.

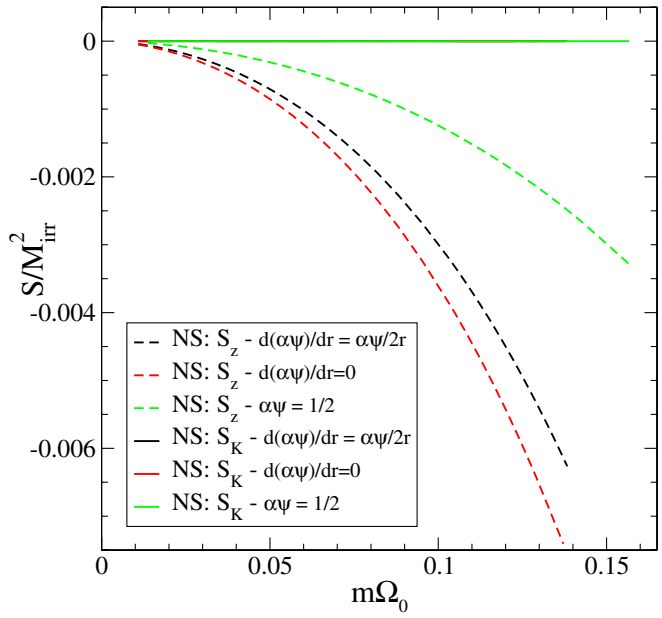

FIG. 9 (color online). Quasilocal spin for a true nonspinning (NS) black hole in an equal-mass binary along the sequence of circular orbits, parametrized by the orbital angular velocity. The same six cases are plotted as in the inset of Fig. 7. Note that here $S_K = 0$ by construction.

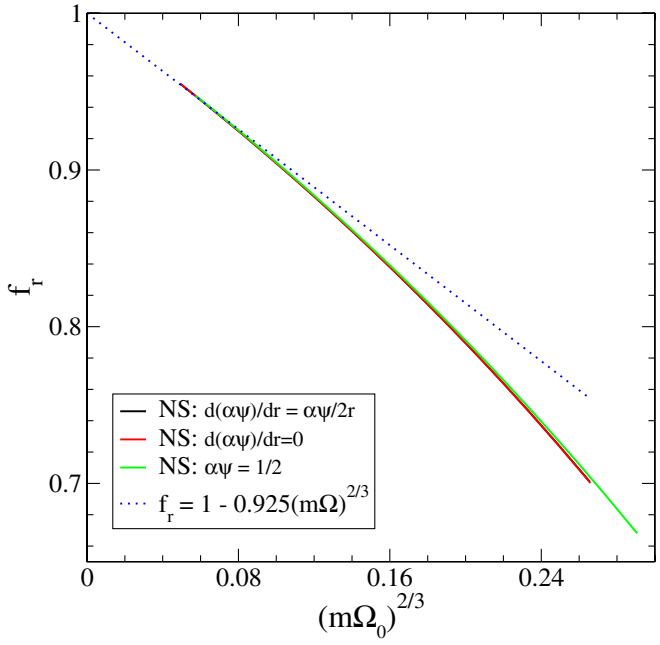

FIG. 10 (color online). Rotation parameter $f_r = \Omega_r/\Omega_0$ along the sequence of nonspinning (NS) black holes, parametrized by the 2/3-power of the orbital angular velocity. The dotted line plots the fit to f_r through the term of order $(m\Omega_0)^{2/3}$.

separations larger than ISCO, we see that, in terms of S_z, the spin does not exceed 0.4% of maximal rotation.

In Fig. 10, we plot the value of the rotation fraction $f_r = \Omega_r/\Omega_0$ as a function of $(m\Omega_0)^{2/3}$. To leading order, we expected $f_r = 1$ and that, to model nonrotating black holes, we needed to set the excision boundary conditions on ${\beta_\parallel}^i$ so as to "unrotate" the black hole from the case of corotation when ${\beta_\parallel}^i = 0$. We might then expect that at higher order we would find $f_r = \Omega_B/\Omega_0 \approx \Omega_T/\Omega_0$. However, comparing f_r in Fig. 10 to Ω_B/Ω_0 in Fig. 5 we see that f_r is significantly smaller. In terms of the previous physical interpretation of the excision boundary conditions for nonspinning holes, this implies that we need to unrotate the black hole by less than the corotation rate. Currently, we do not have a theoretical interpretation for the value of f_r seen in Fig. 10. If we assume that an expansion in terms of $m\Omega_0$ takes the same functional form as Ω_T/Ω_0 in Eq. (56), we find that f_r is well fit by

$$f_r = 1 - 0.925(m\Omega_0)^{2/3} + 0.36(m\Omega_0) - 1.4(m\Omega_0)^{4/3}. \tag{58}$$

We note, however, that f_r can also be well fit by a function that includes a term of order $(m\Omega_0)^{1/3}$.

C. Results for nonspinning binaries

In Ref. [5], we carefully examined the case of equal-mass nonspinning binaries, but the initial-data sets were constructed using the method for defining nonspinning

black holes that is correct only to leading order. Because our improved approach does yield a different spin for the resulting black holes, we reexamine the physical content of these configurations. In the previous section, we computed the sequence of circular orbits for truly nonspinning binaries (cf. Fig. 8). In Figs. 11–13, we plot parameters along the sequence of nonspinning binaries defined using the Komar-mass condition. In each case, we compare our initial-data sequences to the effective one body (EOB) post-Newtonian results [5,10] at first, second, and third post-Newtonian order, to the results of an earlier initial-data method [9], and to the results based on the leading-order method of defining nonspinning black holes. While the difference between our improved numerical results and those based on the leading-order method are not dramatic, they do become significant at small separations.

The most remarkable change produced by the improved method is seen in Fig. 11 which plots the dimensionless binding energy as a function of the dimensionless total angular momentum. Using the leading-order method, the sequence did not approximate a cusp at the ISCO as we would have expected. However, the improved data clearly approximates a cusp. In Ref. [5], we pointed out that we did not understand why our nonspinning data lacked this feature. We now understand that the approximate cusp is a necessary feature of a sequence that is in good agreement with the EP method. This can be seen by looking at Figs. 6 and 8 and considering the behavior near the inflection point of Fig. 8 that defines the ISCO for the EP method. In fact, a

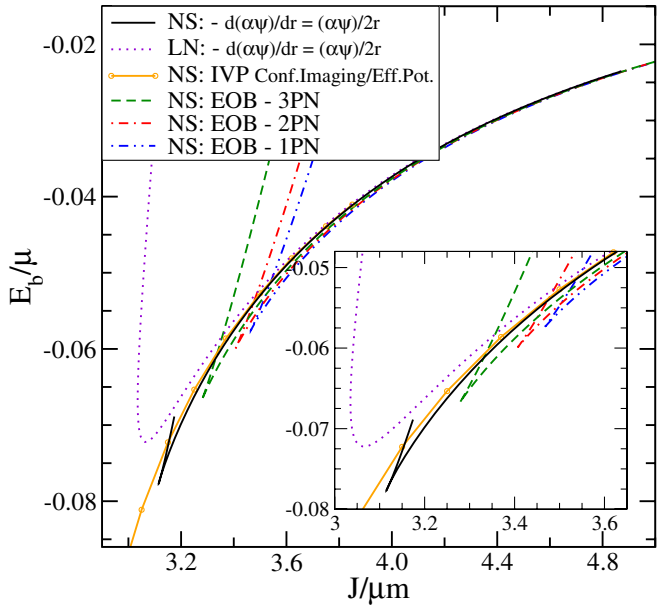

FIG. 11 (color online). Binding energy vs total angular momentum along the sequence of *nonspinning* (NS) equal-mass black holes (as defined by the Komar-mass condition). For comparison, the leading-order nonspinning (LN) results from our earlier work [5] are included, as well as results from Refs. [9,10].

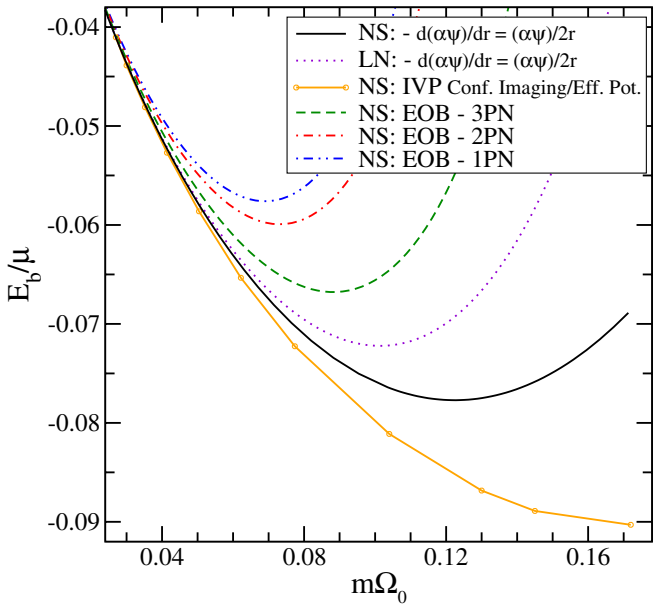

FIG. 12 (color online). Binding energy vs orbital frequency along the sequence of *nonspinning* (NS) equal-mass black holes (as defined by the Komar-mass condition). Lines are labeled as in Fig. 11.

sequence of circular orbits defined by the EP method necessarily has the minima in E_b/μ and $J/\mu m$ coincide, resulting in an exact cusp in the sequence at ISCO.

We can also reexamine how well the improved nonspinning data agrees with the thermodynamic identity of Eq. (41). The third column of Table I shows $M_{\rm irr}$ along a

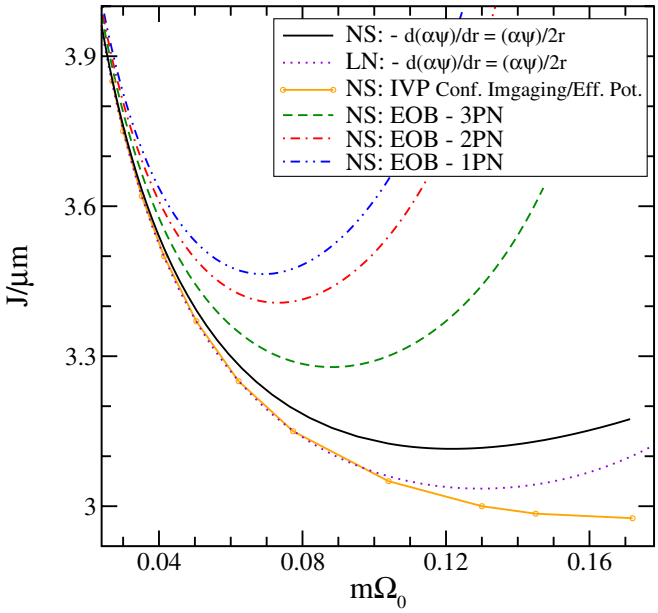

FIG. 13 (color online). Total angular momentum vs orbital frequency along the sequence of *nonspinning* (NS) equal-mass black holes (as defined by the Komar-mass condition). Lines are labeled as in Fig. 11.

sequence of nonspinning equal-mass binaries in circular orbit constructed using the Komar-mass condition. Comparing to the results of the second column for the corresponding case of corotation, we see that the new approach for defining nonspinning binaries yields results that are comparable in magnitude. Also, the variation in $M_{\rm irr}$ is much smaller than those seen in leading-order nonspinning data of the last column.

Finally, it is interesting to reconsider the sequence of nonspinning circular orbits constructed by the EP method. Recalling that an exact stationary solution of Einstein's equations for a black-hole binary can only be found if the black holes are in corotation, we should examine again how well the Komar-mass condition and the EP method agree in their predictions of circular orbits. From Fig. 8, we see that the sequences of circular orbits defined by the two methods nearly coincide except for the regime near the ISCO. For a more quantitative comparison, we can again examine the relative error in the Komar-mass condition. Figure 14 displays this error for the case of nonspinning equal-mass binaries plotted against the dimensionless orbital angular velocity. The magnitude of the relative error is comparable to that of the corotating case plotted in Fig. 2.

We have also examined how well the sequence of nonspinning circular orbits constructed by the EP method agrees with the thermodynamic identity of Eq. (41). As with the corotating case, we use the freedom to define the fundamental length scale along the sequence to enforce Eq. (42). Then the deviation in $M_{\rm irr}$ along the sequence is a measure of how well the thermodynamic identity is satisfied. As with the case of corotation, we find that the variation in the mass is smaller along the EP sequence than in the Komar-mass sequence. However, the variations are *not* as small as seen in the corotating EP sequence. While the variation in the corotating EP sequence were consistent with truncation error, the variations in the nonspinning EP sequence are consistently larger by a factor of about five and the increase in the mass appears to be systematic and significant.

This result should not be surprising since the thermodynamic identity (41) we are testing has only been defined for the case of corotating binaries. What is remarkable is that this identity is satisfied so well for the case of nonspinning black holes.

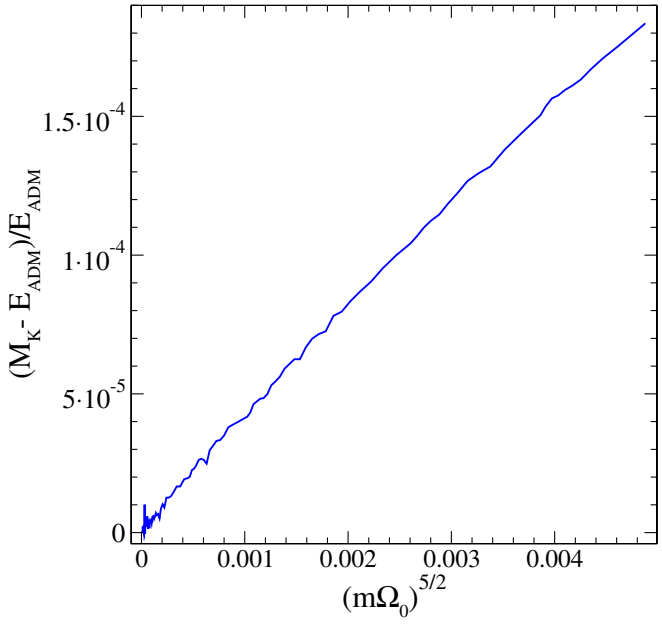

FIG. 14 (color online). Violation of the Komar-mass condition when the effective-potential method is used to determine the sequence of circular orbits. Here, *nonspinning* (NS) equal-mass binaries are considered, and the sequence is parametrized by the orbital angular momentum.

VI. DISCUSSION

Our purpose in this paper has been to explore the spins of black holes in equal-mass binaries in order to verify that the corotating and nonspinning cases were being modeled correctly, and also to explore the assumptions being used to identify configurations that are in circular orbits. In the process of doing this, we have discovered that the assumptions made in the first attempt to construct nonspinning equal-mass binaries (using the quasiequilibrium approach described in this paper) [5] were not leading to sufficiently accurate representations of nonspinning binaries. However, the same quasilocal techniques used to measure the spins of the black holes can also be used to define a new approach for constructing nonspinning black-hole binaries,

TABLE II. Parameters of the ISCO configuration for *nonspinning* equal-mass black holes. Results for the ISCO are given for three different choices of the lapse boundary condition with circular orbits defined by the Komar-mass ansatz and for a single lapse boundary condition with circular orbits defined by the EP method. For comparison, the lower part of the table lists results of Refs. [9–11]; "Conf. Imag." [9] represents data derived from previous numerical initial-data sets; "PN standard" [11] represents a post-Newtonian expansion in the standard form without use of the EOB-technique.

Lapse BC	ISCO type	$m\Omega_0$	E_b/m	J/m^2
$\frac{d(\alpha\psi)}{dr}=0$	Komar	0.122	−0.0194	0.779
$\frac{d(\alpha\psi)}{dr}=\frac{\alpha\psi}{2r}$	Komar	0.122	−0.0194	0.779
	EP	0.121	−0.0193	0.780
$\alpha\psi=\frac{1}{2}$	Komar	0.124	−0.0195	0.778
Conf. Imag.		0.166	−0.0225	0.744
1PN EOB		0.0692	−0.0144	0.866
2PN EOB		0.0732	−0.0150	0.852
3PN EOB		0.0882	−0.0167	0.820
1PN standard		0.5224	−0.0405	0.621
2PN standard		0.1371	−0.0199	0.779
3PN standard		0.1287	−0.0193	0.786

and this approach has produced excellent results. A detailed description of the new results is found in Sec. V C and in Appendix C.

For completeness, we also include tables and figures that detail the ISCO configurations for both corotating and nonspinning cases. Table II displays the new results for ISCO configurations for nonspinning equal-mass binaries. These have changed considerably as is evident by examining these same parameters plotted in Figs. 15–17. In these figures, the previous nonspinning results are labeled as LN: QE and the new results as NS: QE. To facilitate direct comparison, we also include Table III which displays the ISCO result for corotating equal-mass binaries. In both cases, we include results obtained using the three choices for the lapse boundary condition given in Eq. (33) and with circular orbits determined using the Komar-mass condition. Both tables also include a single ISCO model where the circular orbit is determined using the EP method. We include the results only for the lapse boundary condition in Eq. (33b) because locating an ISCO model within the EP approach is very expensive computationally and the results are not sufficiently different from those obtained via the Komar-mass condition to warrant the expense.

We think it worth noting that the value in considering the ISCO parameters is questionable. The ISCO, of course, can only be defined when the effects of radiation reaction are ignored so that the dynamics is conservative. The effects of radiation reaction are certainly not small for equal-mass binaries near ISCO, and so the physical value of locating the ISCO is limited at best. However, the ISCO is a well-defined, unique point in a sequence of (quasi)circular orbits and so has value as a point of comparison between various methods. It also has value in that it marks the regime where

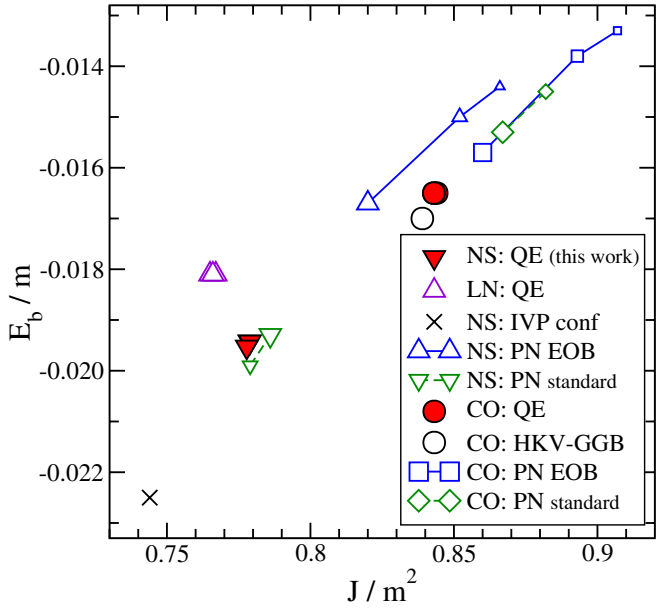

FIG. 15 (color online). ISCO configuration for nonspinning (NS) binary black holes, computed with three different lapse boundary conditions. For comparison, the leading-order nonspinning (LN) and corotating (CO) binary black holes from our earlier work [5] are included, as well as results of Refs. [8–11]. For post-Newtonian calculations the size of the symbol indicates the order, the largest symbol being 3PN. "PN standard" [11] represents a PN expansion in the standard form without use of the EOB technique (only 2PN and 3PN are plotted).

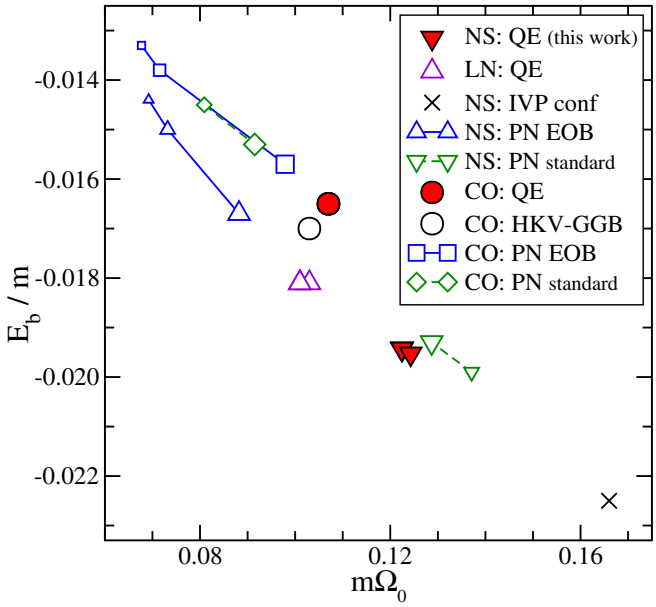

FIG. 16 (color online). ISCO configuration for nonspinning (NS) binary black holes, computed with three different choices of the lapse boundary condition. Symbols as in Fig. 15.

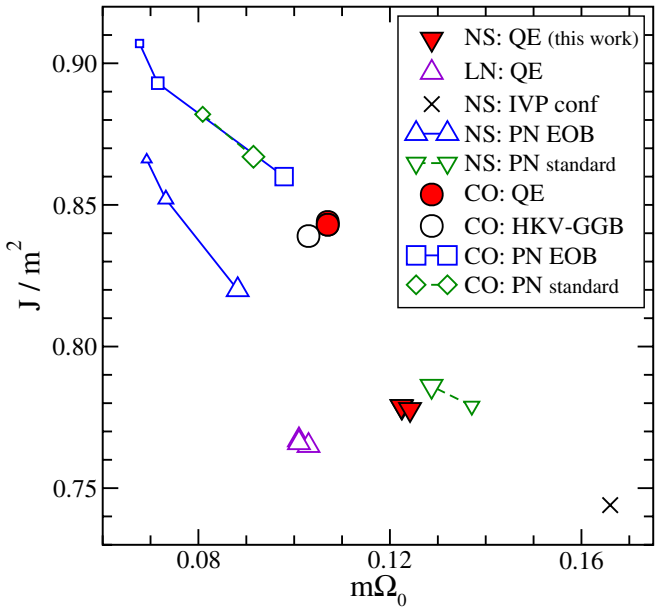

FIG. 17 (color online). ISCO configuration for nonspinning (NS) binary black holes, computed with three different choices of the lapse boundary condition. Symbols as in Fig. 15.

TABLE III. Parameters of the ISCO configuration for *corotating* equal-mass black holes. Results for the ISCO are given for three different choices of the lapse boundary condition with circular orbits defined by the Komar-mass ansatz and for a single lapse boundary condition with circular orbits defined by the EP method. Layout as in Table II.

Lapse BC	ISCO type	$m\Omega_0$	E_b/m	J/m^2
$\frac{d(\alpha\psi)}{dr}=0$	Komar	0.107	−0.0165	0.844
$\frac{d(\alpha\psi)}{dr}=\frac{\alpha\psi}{2r}$	Komar	0.107	−0.0165	0.843
	EP	0.104	−0.0163	0.845
$\alpha\psi=\frac{1}{2}$	Komar	0.107	−0.0165	0.843
HKV-GGB		0.103	−0.017	0.839
1PN EOB		0.0667	−0.0133	0.907
2PN EOB		0.0715	−0.0138	0.893
3PN EOB		0.0979	−0.0157	0.860
1PN standard		0.5224	−0.0405	0.621
2PN standard		0.0809	−0.0145	0.882
3PN standard		0.0915	−0.0153	0.867

the quasiequilibrium approximations have clearly broken down.

In addition to yielding improved initial data for nonspinning equal-mass black-hole binaries, our investigations have shown that the application of quasilocal methods for determining the spins of black holes in binary systems yield remarkably good results. For the case of corotating binaries, we have shown that the quasilocal spin measured for the individual black holes is in excellent agreement with the theoretical expectation for the spin. However, a nagging question remains with regard to the computation of quasilocal spins. This question is associated with the meaning of ''approximate solutions'' of Killing's equation when no true symmetry exists. This is an issue we hope to examine further. We note that, during the preparation of this manuscript, Schnetter *et al.* [61] have also raised this issue.

Concerning the theoretical expectation for the spin, we note that the leading-order result, obtained by assuming that a corotating black hole rotates with an angular velocity equal to the orbital angular velocity of the binary, is not adequate. Using Alvi's [58] leading-order correction to the rate at which a tidal distortion produced by an orbiting star travels around a black hole, we have deduced an improved prediction for the spin of a corotating black hole. It would be useful if a higher-order calculation of Alvi's tidal distortion rotation rate were available. The effect of the corrected rotation rate on post-Newtonian models of corotating binaries should also be considered, especially when higher-order spin-orbit and spin-spin interaction terms become available.

Finally, we note that there is remarkably good agreement between sequences of circular orbits defined via the Komar-mass ansatz and by the EP method. It is natural to ask which method should be used to locate configurations in circular orbit. As described in Sec. IV A, we find that the thermodynamic identity (41) of Friedman *et al.* [29] that applies to corotating binaries in circular orbits is satisfied much more closely by models defined by the EP method than those that satisfy the Komar-mass ansatz. While the EP method yields deviations in the one free quantity ($M_{\rm irr}$) that are 2 orders of magnitude smaller than the Komar-mass condition, the deviations produced by either approach are very small. From a practical perspective, applying the EP method is quite expensive computationally since it requires finding the minima of a ''function'' that is itself defined by root-finding methods. For most applications, it is hard to justify this additional cost.

Perhaps more important than the issue of which approach is better is the fact that both methods agree so well also for the case of nonspinning binaries *and* that both methods are in good agreement with the thermodynamic identity of Eq. (41). This is surprising because the identity was intended to apply only in the case of corotating black-holes binaries. If the agreement only held at large separation, it would be reasonable to assume that the identity held because strong-field effects were simply small in this regime. However, the agreement holds at all separations which suggests that there may be something more fundamental at work.

ACKNOWLEDGMENTS

We would like to thank Bernard Whiting and Clifford Will for useful discussions. This work was supported in part by NSF Grant No. PHY-0244906 to the California Institute of Technology. Computations were performed on the Wake Forest University DEAC Cluster.

APPENDIX A: SOLVING KILLING'S EQUATION

A straightforward method for finding Killing vectors was outlined by Dreyer *et al.* [27]. Here we outline that method as we have implemented it to locate Killing vectors on a surface $\mathcal{S}$ with S^2 topology. In our case, $\mathcal{S}$ is a coordinate sphere in the flat conformal 3-geometry. Following Eq. (27), our metric is denoted h_{ij} and it is conformally related to $\tilde{h}_{ij}$ which is the metric of a coordinate 2-sphere with radius r. Following Ref. [27], we let ξ^i denote a Killing vector on $(\mathcal{S}, h_{ij})$ and define a two-form $L_{ij} \equiv D_i \xi_j$, where D_i is the covariant derivative compatible with h_{ij}. Now, the Killing equation can be written simply as

$$L_{(ij)} = 0. \tag{A1}$$

However, instead of solving the Killing equation directly, Dreyer *et al.* propose to solve the *Killing transport equations*:

$$D_i \xi_j = L_{ij}, \tag{A2a}$$
$$D_i L_{jk} = {}^2R_{kji}{}^{\ell}\,\xi_{\ell}, \tag{A2b}$$

for the two-form L_{ij} and vector ξ^i. Here, ${}^2R_{kji}{}^{\ell}$ is the Riemann tensor associated with h_{ij}. Note that Eq. (A2b) follows from Eq. (A2a) by using various symmetries of Riemann *and assuming that* ξ^i *is a Killing vector* (i.e. that $D_{(i}\xi_{j)} = 0$).

The central idea in using Eqs. (A2) to find Killing vectors is to note that the Killing transport equations act as a linear map on the set of variables (ξ_i, L_{ij}). In particular, consider integrating these equations along some path from point p to point q. If $(\mathcal{S}, h_{ij})$ has solutions of the Killing Eq. (A1), and if $(\xi_i, L_{ij})|_p$ come from one of these Killing solutions, then integrating the Killing transport equations along the path will yield $(\xi_i, L_{ij})|_q$ which comes from the *same* Killing vector.

Since our surface $\mathcal{S}$ is 2-dimensional, it follows that

$${}^2R_{ijk\ell} = \tfrac{1}{2}\,{}^2R\,\epsilon_{ij}\epsilon_{k\ell}, \tag{A3}$$

$$L_{ij} = L\epsilon_{ij}, \tag{A4}$$

where ${}^2R$ is the 2-dimensional Ricci scalar associated with h_{ij} and L is an oriented scalar on $\mathcal{S}$. For our particular metric,

$$\mathrm{d}s^2 = \psi^4 r^2(\mathrm{d}\theta^2 + \sin^2\theta \mathrm{d}\phi^2), \tag{A5}$$

the Killing transport equations can be written in spherical coordinate components as

$$\frac{\partial \xi_\theta}{\partial \theta} = 2\xi_\theta \partial_\theta \ln\psi - \frac{2}{\sin^2\theta}\xi_\phi \partial_\phi \ln\psi, \tag{A6a}$$
$$\frac{\partial \xi_\phi}{\partial \theta} = \cot\theta \xi_\phi + L\psi^4 r^2 \sin\theta + 2\xi_\theta \partial_\phi \ln\psi + 2\xi_\phi \partial_\theta \ln\psi, \tag{A6b}$$
$$\frac{\partial L}{\partial \theta} = -\left(\frac{1}{\psi^4 r^2} - 2D^i D_i \ln\psi\right)\frac{1}{\sin\theta}\xi_\phi, \tag{A6c}$$

$$\frac{\partial \xi_\theta}{\partial \phi} = \cot\theta \xi_\phi - L\psi^4 r^2 \sin\theta + 2\xi_\theta \partial_\phi \ln\psi + 2\xi_\phi \partial_\theta \ln\psi, \tag{A7a}$$
$$\frac{\partial \xi_\phi}{\partial \phi} = -\sin\theta\cos\theta\xi_\theta - 2\sin^2\theta\xi_\theta \partial_\theta \ln\psi + 2\xi_\phi \partial_\phi \ln\psi, \tag{A7b}$$
$$\frac{\partial L}{\partial \phi} = \left(\frac{1}{\psi^4 r^2} - 2D^i D_i \ln\psi\right)\sin\theta\xi_\theta. \tag{A7c}$$

It is particularly convenient to compute these quantities in terms of a basis set $(\bar\theta, \bar\phi)$ which is orthonormal as defined on the *unit* 2-sphere. We find then that

$$\xi_{\bar\theta} \equiv \xi_\theta \quad \text{and} \quad \xi_{\bar\phi} \equiv \frac{1}{\sin\theta}\xi_\phi. \tag{A8}$$

The Killing transport equations then take the form

$$\frac{\partial \xi_{\bar\theta}}{\partial \theta} = 2\xi_{\bar\theta}({}_{\mathrm{s}}\vec\nabla \ln\psi)_{\bar\theta} - 2\xi_{\bar\phi}({}_{\mathrm{s}}\vec\nabla \ln\psi)_{\bar\phi}, \tag{A9a}$$
$$\frac{\partial \xi_{\bar\phi}}{\partial \theta} = L\psi^4 r^2 + 2\xi_{\bar\theta}({}_{\mathrm{s}}\vec\nabla \ln\psi)_{\bar\phi} + 2\xi_{\bar\phi}({}_{\mathrm{s}}\vec\nabla \ln\psi)_{\bar\theta}, \tag{A9b}$$
$$\frac{\partial L}{\partial \theta} = -\frac{(1 - 2{}_{\mathrm{s}}\nabla^2 \ln\psi)}{\psi^4 r^2}\xi_{\bar\phi}, \tag{A9c}$$

$$\frac{\partial \xi_{\bar\theta}}{\partial \phi} = \cos\theta\xi_{\bar\phi} - L\psi^4 r^2 \sin\theta + 2\sin\theta\xi_{\bar\theta}({}_{\mathrm{s}}\vec\nabla \ln\psi)_{\bar\phi} + 2\sin\theta\xi_{\bar\phi}({}_{\mathrm{s}}\vec\nabla \ln\psi)_{\bar\theta}, \tag{A10a}$$
$$\frac{\partial \xi_{\bar\phi}}{\partial \phi} = -\cos\theta\xi_{\bar\theta} - 2\sin\theta\xi_{\bar\theta}({}_{\mathrm{s}}\vec\nabla \ln\psi)_{\bar\theta} + 2\sin\theta\xi_{\bar\phi}({}_{\mathrm{s}}\vec\nabla \ln\psi)_{\bar\phi}, \tag{A10b}$$
$$\frac{\partial L}{\partial \phi} = \frac{(1 - 2{}_{\mathrm{s}}\nabla^2 \ln\psi)}{\psi^4 r^2}\sin\theta\xi_{\bar\theta}, \tag{A10c}$$

where ${}_{\mathrm{s}}\vec\nabla$ and ${}_{\mathrm{s}}\nabla^2$ are the usual gradient and Laplacian operators defined for the unit 2-sphere.

Let $\mathbf{V}$ denote the vector of quantities

$$\mathbf{V} = \begin{pmatrix} \xi_{\bar\theta} \\ \xi_{\bar\phi} \\ L \end{pmatrix}. \tag{A11}$$

Using fourth-order Runge-Kutta, we integrate Eqs. (A10) around a closed path from $\phi = 0$ to $\phi = 2\pi$ along the equator $\theta = \frac{\pi}{2}$ starting with three different values for $\mathbf{V}|_{(\phi=0)}$: (1,0,0), (0,1,0), and (0,0,1). The three resulting vectors, $\mathbf{V}|_{(\phi=2\pi)}$ can be used to construct a matrix $\mathbf{M}$ that represents the action of the linear map of the Killing transport equations on any vector:

$$\mathbf{V}|_{(\phi=2\pi)} = \mathbf{M}\cdot\mathbf{V}|_{(\phi=0)}. \tag{A12}$$

If $\mathbf{V}|_{(\phi=0)}$ is derived from a Killing vector, then Eq. (A12) will yield $\mathbf{V}|_{(\phi=2\pi)} = \mathbf{V}|_{(\phi=0)}$. So, if $(\mathcal{S}, h_{ij})$ possesses a global solution of the Killing equation, it will be associated with a *unit eigenvalue* of $\mathbf{M}$ and the associated eigenvector will be derived from that Killing vector. In general, $(\mathcal{S}, h_{ij})$ will not possess a Killing vector and $\mathbf{M}$ will have no unit eigenvalues. One could proceed to construct an "approximate Killing vector" by using an eigenvalue that is sufficiently close to unity.

However, for the corotating and nonspinning black-hole binary initial data we consider in this paper, the conformal factor possesses a reflection symmetry through the plane of the orbit. We thus find that the eigenvector (0,1,0) always has unit eigenvalue when we integrate along the equator.[2]

[2]This is most easily seen by writing the Killing transport equations in terms of an orthonormal basis set $(\hat\theta, \hat\phi)$ defined with respect to the full metric h_{ij} so that $\xi_{\hat\theta} \equiv \frac{1}{\psi^2 r}\xi_\theta$ and $\xi_{\hat\phi} \equiv \frac{1}{\psi^2 r\sin\theta}\xi_\phi$.

Unfortunately, this vector does not necessarily represent a global Killing vector on $\mathcal{S}$.

Our pseudospectral code for solving the constraint equations represents quantities on the excision boundaries in terms of spherical harmonic decompositions. To proceed we need to populate the collocation points (grid points) of the spectral grid with values for $\mathbf{V}$ obtained by propagating the eigenvector (0,1,0) at $(\theta = \frac{\pi}{2}, \phi = 0)$ to all of these points via the Killing transport equations. If our starting vector were constructed from a global Killing vector, then the path we take to each of these points would not matter. However, since we do not in general have a true global Killing vector, we must specify how we populate the grid points.

First, we integrate Eqs. (A10) to populate values along the equator ($\theta = \frac{\pi}{2}$) wherever they are needed, integrating from $\phi = 0$ to $\phi = 2\pi$. For each line of colatitude containing collocation points, we integrate Eqs. (A9a)–(A9c) starting with the known values at the equator. All integrations are performed using fourth-order Runge-Kutta. With values for $\xi_{\hat{\theta}}$ and $\xi_{\hat{\phi}}$ at all collocation points, we can construct a vector spherical harmonic representation of our solution over the entire surface $\mathcal{S}$. All that remains is to normalize the Killing vector and check to see if we have a true Killing vector.

A rotational Killing vector (as we are trying to construct) is normalized so that its affine length is 2π. Consider a path parametrized by t and defined by

$$\frac{\partial\theta}{\partial t} = \frac{1}{\psi^4 r^2}\xi_{\bar{\theta}}, \tag{A13a}$$

$$\frac{\partial\phi}{\partial t} = \frac{1}{\psi^4 r^2 \sin\theta}\xi_{\bar{\phi}}. \tag{A13b}$$

We integrate from some starting location $(\theta, \phi)|_0$ with $t = 0$ until the path closes at the starting point. If ξ is not properly normalized, then the final value of t_f will not be 2π. However, using t_f we can rescale $\vec{\xi}$ so that it does have an affine length of 2π. In practice, we normalize the solution by integrating along the equator, then check that the solution is correctly normalized to within truncation error for several different integral paths starting at $\phi = 0$ and various initial values for θ.

There are many possible ways of determining whether or not our solution is a global solution of the Killing equation. For simplicity, we check the following set of scalar conditions that must be satisfied everywhere if our solution is a true Killing vector of $(\mathcal{S}, h_{ij})$:

$$\xi^i D_i L = 0, \tag{A14a}$$

$$D_i \xi^i = 0, \tag{A14b}$$

$$\epsilon^{ij} D_i \xi_j = 2L. \tag{A14c}$$

In terms of our basis defined by Eq. (A8), these become

$$\frac{1}{\psi^4 r^2}(\xi_{\bar{\theta}}({}_s\vec{\nabla}L)_{\bar{\theta}} + \xi_{\bar{\phi}}({}_s\vec{\nabla}L)_{\bar{\phi}}) = 0, \tag{A15a}$$

$$\frac{1}{\psi^4 r^2}\,{}_s\vec{\nabla}\cdot\vec{\xi} = 0, \tag{A15b}$$

$$\frac{1}{\psi^4 r^2}\,{}_s\vec{\nabla}\times\vec{\xi} = 2L, \tag{A15c}$$

and ${}_s\vec{\nabla}\cdot$ and ${}_s\vec{\nabla}\times$ are the usual divergence and twist operators defined for the unit 2-sphere. We find that these identities are never satisfied for our solutions although the residuals seem "small" and decrease in size as the separation between the black holes increases. Because we have not yet found any way to meaningfully normalize the values of the residuals, we do no bother to report their values here.

We do note that, because we represent $\vec{\xi}$ in terms of vector spherical harmonics, it is possible to filter the coefficients in the vector spherical harmonic expansion to ensure that it is divergenceless. That is, we can, *a posteriori* guarantee that Eq. (A15b) is satisfied. However, this does not change the other diagnostics. All of the results presented in this paper that depend on solutions of the Killing equation have been filtered in this way. We note that this filtering has a negligible effect on all measured quantities.

We conclude this Appendix by noting that our solutions of the Killing equation are "approximate Killing vectors" in some sense that is not at all well defined. In all cases, we find that our approximate Killing vector is very similar to the corresponding solution on the unit 2-sphere. These are conformal Killing vectors of $(\mathcal{S}, h_{ij})$ as written down in Eqs. (39a)–(39c). We leave it to future work to more rigorously define the meaning of these "approximate Killing vectors."

Finally, we note that, during the preparation of this manuscript, Schnetter *et al.* [61] have shown that, when a divergence-free approximate Killing vector is used to define the quasilocal angular momentum, as in Eq. (38), then it is gauge invariant. Therefore, they suggest that such a divergence-free approximate Killing vector "can be viewed as an *ersatz* axial symmetry vector even in the absence of axisymmetry."

APPENDIX B: COROTATING SEQUENCE

In this Appendix, we list the numerical results for corotating equal-mass black holes in a quasicircular orbit as defined by the Komar ansatz. We have assumed conformal flatness, maximal slicing, and used Eq. (33b) for the lapse boundary condition on both excision surfaces. The data is scaled relative to the total and reduced masses (m and μ) defined with respect to the irreducible mass of the apparent horizons $M_{\rm irr}$.

In Table IV, d and Ω_0 are, respectively, the separation of the centers of the excised regions and the orbital angular velocity measured in "coordinate units." These values for

TABLE IV. Sequence of corotating equal-mass black holes on circular orbits satisfying the Komar ansatz. The ISCO is at separation $d \sim 8.28$.

d	Ω_0	$m\Omega_0$	E_b/μ	$J/\mu m$	ℓ/m	$S_z/M_{\rm irr}^2$	$S_K/M_{\rm irr}^2$
40	0.005 296 6	0.010 90	−0.023 318 3	4.9120	22.87	0.021 48	0.021 50
35	0.006 421 2	0.013 27	−0.026 326 5	4.6620	20.23	0.026 09	0.026 12
30	0.008 008 3	0.016 65	−0.030 193 0	4.4019	17.58	0.032 64	0.032 67
29	0.008 405 0	0.017 50	−0.031 100 8	4.3488	17.04	0.034 28	0.034 31
28	0.008 835 4	0.018 42	−0.032 062 2	4.2953	16.51	0.036 06	0.036 10
27	0.009 303 9	0.019 43	−0.033 081 6	4.2414	15.97	0.038 00	0.038 04
26	0.009 815 1	0.020 54	−0.034 164 2	4.1872	15.43	0.040 12	0.040 17
25	0.010 375	0.021 75	−0.035 315 3	4.1328	14.89	0.042 45	0.042 50
24	0.010 990	0.023 09	−0.036 540 9	4.0781	14.35	0.045 01	0.045 07
23	0.011 667	0.024 57	−0.037 847 6	4.0233	13.81	0.047 85	0.047 91
22	0.012 418	0.026 22	−0.039 242 3	3.9684	13.26	0.050 99	0.051 06
21	0.013 252	0.028 06	−0.040 732 5	3.9135	12.72	0.054 49	0.054 57
20	0.014 183	0.030 12	−0.042 326 2	3.8587	12.17	0.058 41	0.058 50
19	0.015 227	0.032 45	−0.044 031 3	3.8043	11.62	0.062 82	0.062 93
18	0.016 406	0.035 11	−0.045 855 5	3.7503	11.06	0.067 82	0.067 94
17	0.017 744	0.038 14	−0.047 805 6	3.6971	10.50	0.073 52	0.073 66
16	0.019 273	0.041 64	−0.049 885 7	3.6450	9.943	0.080 07	0.080 24
15	0.021 031	0.045 71	−0.052 095 6	3.5944	9.377	0.087 65	0.087 85
14.5	0.022 012	0.048 00	−0.053 247 0	3.5699	9.092	0.091 90	0.092 12
14	0.023 070	0.050 49	−0.054 426 7	3.5460	8.807	0.096 50	0.096 74
13.5	0.024 215	0.053 20	−0.055 631 0	3.5229	8.520	0.1015	0.1018
13	0.025 456	0.056 17	−0.056 854 9	3.5006	8.231	0.1070	0.1073
12.5	0.026 804	0.059 42	−0.058 091 2	3.4793	7.941	0.1129	0.1132
12	0.028 273	0.063 00	−0.059 329 8	3.4592	7.649	0.1195	0.1198
11.5	0.029 877	0.066 96	−0.060 556 5	3.4405	7.356	0.1266	0.1271
11	0.031 634	0.071 35	−0.061 752 3	3.4234	7.060	0.1346	0.1350
10.5	0.033 564	0.076 25	−0.062 890 9	3.4082	6.762	0.1434	0.1439
10	0.035 689	0.081 74	−0.063 936 4	3.3952	6.462	0.1532	0.1538
9.5	0.038 037	0.087 92	−0.064 840 1	3.3848	6.159	0.1642	0.1649
9	0.040 638	0.094 93	−0.065 534 8	3.3775	5.853	0.1765	0.1773
8.9	0.041 191	0.096 44	−0.065 641 0	3.3765	5.792	0.1792	0.1800
8.8	0.041 757	0.098 00	−0.065 734 5	3.3756	5.731	0.1819	0.1828
8.7	0.042 334	0.099 60	−0.065 814 2	3.3749	5.669	0.1847	0.1856
8.6	0.042 923	0.1012	−0.065 879 1	3.3744	5.607	0.1876	0.1885
8.5	0.043 526	0.1029	−0.065 928 2	3.3740	5.545	0.1905	0.1915
8.4	0.044 141	0.1047	−0.065 960 3	3.3738	5.483	0.1936	0.1945
8.35	0.044 453	0.1055	−0.065 969 5	3.3737	5.451	0.1951	0.1961
8.3	0.044 769	0.1064	−0.065 974 1	3.3738	5.420	0.1967	0.1977
8.25	0.045 089	0.1074	−0.065 973 8	3.3738	5.389	0.1982	0.1993
8.2	0.045 412	0.1083	−0.065 968 5	3.3739	5.358	0.1998	0.2009
8.1	0.046 068	0.1102	−0.065 941 9	3.3743	5.295	0.2031	0.2042
8	0.046 738	0.1121	−0.065 892 9	3.3748	5.232	0.2065	0.2076

d and Ω, together with the coordinate radius of the excision sphere $r = 0.785\,798\,137\,1$, provide all parameters necessary to reproduce the data in Table IV. The remaining quantities are dimensionless. $m\Omega_0$ is the orbital angular velocity of the binary system as measured at infinity. E_b/μ is the dimensionless binding energy of the system with E_b defined as $E_b \equiv E_{\rm ADM} - m$. $J/\mu m$ is the dimensionless total ADM angular momentum of the binary system as measured at infinity. ℓ/m is the dimensionless proper separation between the two excision surfaces as measured on the initial-data slice.[3] Finally, $S_z/M_{\rm irr}^2$ and $S_K/M_{\rm irr}^2$ are two measures of the dimensionless spin of one of the black holes. S_z is defined using the flat-space Killing vector and S_K is defined using the approximate Killing vector.

[3]Note that the value of ℓ listed in Tables IV and V of Ref. [5] were in error. The corrected values for the corotating case, and correct values for the true nonspinning case, are given in the following tables.

APPENDIX C: NONSPINNING SEQUENCE

In this Appendix, we list the numerical results for nonspinning equal-mass black holes in a quasicircular orbit as defined by the Komar ansatz. We have assumed conformal flatness, maximal slicing, and used Eq. (33b) for the lapse boundary condition on both excision surfaces. The data is scaled relative to the total and reduced masses (m and μ) defined with respect to the irreducible mass of the apparent horizons $M_{\rm irr}$.

In Table V, d and Ω_0 are, respectively, the separation of the centers of the excised regions and the orbital angular velocity measured in "coordinate units." $f_r = \Omega_r/\Omega_0$ is the rotation fraction necessary to obtain a nonspinning black hole. These values for d, Ω, and f_r, together with the coordinate radius of the excision sphere $r = 0.785\,798\,137\,1$, provide all parameters necessary to reproduce the data in Table V. The remaining quantities are dimensionless. $m\Omega_0$ is the orbital angular velocity of the binary system as measured at infinity. E_b/μ is the dimen-

TABLE V. Sequence of nonspinning equal-mass black holes on circular orbits satisfying the Komar ansatz. The ISCO is at separation $d \sim 7.55$.

d	Ω_0	f_r	$m\Omega_0$	E_b/μ	$J/\mu m$	ℓ/m	$S_z/M_{\rm irr}^2$
40	0.005 297 3	0.9551	0.010 90	−0.023 532 9	4.8717	22.87	−0.000 042 06
35	0.006 422 5	0.9485	0.013 27	−0.026 639 6	4.6136	20.24	−0.000 059 74
30	0.008 010 8	0.9396	0.016 65	−0.030 675 1	4.3423	17.58	−0.000 089 63
29	0.008 407 9	0.9374	0.017 50	−0.031 630 4	4.2864	17.05	−0.000 098 13
28	0.008 838 8	0.9351	0.018 43	−0.032 645 8	4.2298	16.51	−0.000 107 7
27	0.009 307 9	0.9326	0.019 43	−0.033 726 8	4.1727	15.98	−0.000 118 7
26	0.009 819 8	0.9299	0.020 54	−0.034 880 0	4.1150	15.44	−0.000 131 2
25	0.010 380	0.9270	0.021 75	−0.036 112 2	4.0568	14.90	−0.000 145 8
24	0.010 996	0.9238	0.023 09	−0.037 431 7	3.9979	14.36	−0.000 162 7
23	0.011 676	0.9203	0.024 57	−0.038 847 3	3.9386	13.82	−0.000 182 5
22	0.012 428	0.9165	0.026 22	−0.040 369 3	3.8786	13.27	−0.000 205 8
21	0.013 264	0.9123	0.028 06	−0.042 009 2	3.8182	12.73	−0.000 233 6
20	0.014 198	0.9077	0.030 13	−0.043 779 9	3.7574	12.18	−0.000 266 9
19	0.015 247	0.9025	0.032 46	−0.045 695 7	3.6962	11.63	−0.000 307 2
18	0.016 431	0.8967	0.035 12	−0.047 772 6	3.6348	11.07	−0.000 356 7
17	0.017 775	0.8903	0.038 16	−0.050 028 0	3.5732	10.52	−0.000 418 0
16	0.019 313	0.8829	0.041 66	−0.052 480 2	3.5118	9.957	−0.000 495 2
15	0.021 085	0.8745	0.045 74	−0.055 147 3	3.4509	9.393	−0.000 594 0
14.5	0.022 075	0.8698	0.048 04	−0.056 566 5	3.4207	9.110	−0.000 653 9
14	0.023 143	0.8647	0.050 53	−0.058 044 8	3.3907	8.825	−0.000 722 6
13.5	0.024 300	0.8593	0.053 26	−0.059 583 0	3.3612	8.539	−0.000 802 0
13	0.025 556	0.8533	0.056 23	−0.061 180 7	3.3321	8.252	−0.000 894 2
12.5	0.026 923	0.8469	0.059 50	−0.062 836 3	3.3036	7.963	−0.001 002
12	0.028 415	0.8399	0.063 10	−0.064 545 7	3.2758	7.673	−0.001 129
11.5	0.030 047	0.8321	0.067 09	−0.066 301 7	3.2490	7.381	−0.001 279
11	0.031 840	0.8236	0.071 51	−0.068 092 2	3.2233	7.087	−0.001 460
10.5	0.033 815	0.8142	0.076 45	−0.069 898 4	3.1991	6.791	−0.001 678
10	0.035 998	0.8036	0.082 00	−0.071 690 7	3.1766	6.493	−0.001 946
9.5	0.038 420	0.7918	0.088 26	−0.073 424 2	3.1565	6.193	−0.002 277
9	0.041 118	0.7785	0.095 38	−0.075 030 3	3.1393	5.891	−0.002 693
8.5	0.044 133	0.7632	0.1035	−0.076 402 9	3.1258	5.585	−0.003 226
8	0.047 516	0.7457	0.1129	−0.077 378 5	3.1172	5.277	−0.003 920
7.9	0.048 241	0.7419	0.1150	−0.077 505 4	3.1162	5.215	−0.004 084
7.8	0.048 984	0.7379	0.1171	−0.077 603 9	3.1154	5.153	−0.004 257
7.7	0.049 745	0.7338	0.1193	−0.077 671 1	3.1149	5.090	−0.004 442
7.65	0.050 132	0.7318	0.1204	−0.077 692 0	3.1148	5.059	−0.004 538
7.6	0.050 524	0.7296	0.1216	−0.077 703 7	3.1148	5.028	−0.004 637
7.55	0.050 921	0.7275	0.1227	−0.077 705 8	3.1148	4.996	−0.004 740
7.5	0.051 323	0.7253	0.1239	−0.077 698 0	3.1149	4.965	−0.004 846
7.4	0.052 140	0.7208	0.1263	−0.077 650 1	3.1154	4.902	−0.005 067
7.3	0.052 978	0.7161	0.1288	−0.077 555 7	3.1163	4.839	−0.005 304

sionless binding energy of the system with E_b defined as $E_b \equiv E_{\rm ADM} - m$. $J/\mu m$ is the dimensionless total ADM angular momentum of the binary system as measured at infinity. ℓ/m is the dimensionless proper separation between the two excision surfaces as measured on the initial-data slice. $S_z/M_{\rm irr}^2$ is the dimensionless spin of one of the black holes where S_z is defined using the flat-space Killing vector. The spin defined using the approximate Killing vector is zero by definition.

[1] F. Pretorius, Phys. Rev. Lett. **95**, 121101 (2005).
[2] M. Campanelli, C. O. Lousto, P. Marronetti, and Y. Zlochower, Phys. Rev. Lett. **96**, 111101 (2006).
[3] J. G. Baker, J. Centrella, D. Il Choi, M. Koppitz, and J. van Meter, Phys. Rev. Lett. **96**, 111102 (2006).
[4] P. Diener, F. Herrmann, D. Pollney, E. Schnetter, E. Seidel, R. Takahashi, J. Thornburg, and J. Ventrella, Phys. Rev. Lett. **96**, 121101 (2006).
[5] G. B. Cook and H. P. Pfeiffer, Phys. Rev. D **70**, 104016 (2004).
[6] G. B. Cook, Phys. Rev. D **65**, 084003 (2002).
[7] E. Gourgoulhon, P. Grandclément, and S. Bonazzola, Phys. Rev. D **65**, 044020 (2002).
[8] P. Grandclément, E. Gourgoulhon, and S. Bonazzola, Phys. Rev. D **65**, 044021 (2002).
[9] G. B. Cook, Phys. Rev. D **50**, 5025 (1994).
[10] T. Damour, E. Gourgoulhon, and P. Grandclément, Phys. Rev. D **66**, 024007 (2002).
[11] L. Blanchet, Phys. Rev. D **65**, 124009 (2002).
[12] A. Komar, Phys. Rev. **113**, 934 (1959).
[13] R. Arnowitt, S. Deser, and C. W. Misner, in *Gravitation: An Introduction to Current Research*, edited by L. Witten (Wiley, New York, 1962), pp. 227–265.
[14] K. Taniguchi and E. Gourgoulhon, Phys. Rev. D **66**, 104019 (2002).
[15] L. B. Szabados, Living Rev. Relativity **7**, 4 (2004), http://www.livingreviews.org/lrr-2004-4
[16] J. D. Brown and J. W. York, Jr., Phys. Rev. D **47**, 1407 (1993).
[17] A. Ashtekar and B. Krishnan, Phys. Rev. D **68**, 104030 (2003).
[18] A. Ashtekar and B. Krishnan, Living Rev. Relativity **7**, 10 (2004), http://www.livingreviews.org/lrr-2004-10.
[19] J. W. York, Jr., Phys. Rev. Lett. **82**, 1350 (1999).
[20] H. P. Pfeiffer and J. W. York, Jr., Phys. Rev. D **67**, 044022 (2003).
[21] A. Lichnerowicz, J. Math. Pures Appl. **23**, 37 (1944).
[22] J. W. York, Jr., Phys. Rev. Lett. **26**, 1656 (1971).
[23] J. W. York, Jr., Phys. Rev. Lett. **28**, 1082 (1972).
[24] G. B. Cook, S. L. Shapiro, and S. A. Teukolsky, Phys. Rev. D **53**, 5533 (1996).
[25] T. W. Baumgarte, G. B. Cook, M. A. Scheel, S. L. Shapiro, and S. A. Teukolsky, Phys. Rev. D **57**, 7299 (1998).
[26] A. Ashtekar, C. Beetle, O. Dreyer, S. Fairhurst, B. Krishnan, J. Lewandowski, and J. Wiśniewski, Phys. Rev. Lett. **85**, 3564 (2000).
[27] O. Dreyer, B. Krishnan, D. Shoemaker, and E. Schnetter, Phys. Rev. D **67**, 024018 (2003).
[28] J. L. Jaramillo, E. Gourgoulhon, and G. A. M. Marugán, Phys. Rev. D **70**, 124036 (2004).
[29] J. L. Friedman, K. Uryū, and M. Shibata, Phys. Rev. D **65**, 064035 (2002).
[30] P. Painlevé, C. R. Acad Sci **173**, 677 (1921).
[31] A. Gullstrand, Ark. Mat. Astron. Fys. **16**, 1 (1922).
[32] K. Martel and E. Poisson, Am. J. Phys. **69**, 476 (2001).
[33] C. Doran, Phys. Rev. D **61**, 067503 (2000).
[34] C. W. Misner, Ann. Phys. (Leipzig) **24**, 102 (1963).
[35] R. W. Lindquist, J. Math. Phys. (N.Y.) **4**, 938 (1963).
[36] D. R. Brill and R. W. Lindquist, Phys. Rev. **131**, 471 (1963).
[37] J. K. Blackburn and S. Detweiler, Phys. Rev. D **46**, 2318 (1992).
[38] S. Detweiler, Phys. Rev. D **50**, 4929 (1994).
[39] J. T. Whelan, W. Krivan, and R. H. Price, Classical Quantum Gravity **17**, 4895 (2000).
[40] J. T. Whelan, C. Beetle, W. Landry, and R. H. Price, Classical Quantum Gravity **19**, 1285 (2002).
[41] C. Klein, Phys. Rev. D **70**, 124026 (2004).
[42] T. Mora and C. M. Will, Phys. Rev. D **69**, 104021 (2004).
[43] R. Rieth, in *Proceedings of the Workshop on Mathematical Aspects of Theories of Gravitation held in Warsaw, 1996*, edited by A. Królak (Polish Academy of Sciences, Institute of Mathematics, Warsaw, 1997), pp. 71–74.
[44] A. Garat and R. H. Price, Phys. Rev. D **61**, 124011 (2000).
[45] J. A. V. Kroon, Phys. Rev. Lett. **92**, 041101 (2004).
[46] W. Tichy, B. Brügmann, M. Campanelli, and P. Diener, Phys. Rev. D **67**, 064008 (2003).
[47] M. Shibata, K. Uryū, and J. L. Friedman, Phys. Rev. D **70**, 044044 (2004).
[48] K. Uryū, F. Limousin, J. L. Friedman, E. Gourgoulhon, and M. Shibata, gr-qc/0511136.
[49] H. P. Pfeiffer, L. E. Kidder, M. A. Scheel, and S. A. Teukolsky, Comput. Phys. Commun. **152**, 253 (2003).
[50] J. B. Boyd, *Chebyshev and Fourier Spectral Methods, 2nd edition* (Dover, New York, 2001), for an online version, see http://www-personal.engin.umich.edu/~jpboyd.
[51] M. Barrett, M. Berry, T. F. Chan, J. Van der Horst, and H. Van der Horst, *Templates for the Solution of Linear Systems: Building Blocks for Iterative Methods* (SIAM, Philadelphia, PA, 1994).
[52] Y. Saad, SIAM J. Sci. Comput. **14**, 461 (1993).
[53] T. W. Baumgarte, Phys. Rev. D **62**, 024018 (2000).
[54] H. P. Pfeiffer, S. A. Teukolsky, and G. B. Cook, Phys. Rev. D **62**, 104018 (2000).
[55] M. L. Skoge and T. W. Baumgarte, Phys. Rev. D **66**, 107501 (2002).

[56] W. Tichy and B. Brügmann, Phys. Rev. D **69**, 024006 (2004).
[57] D. Christodoulou, Phys. Rev. Lett. **25**, 1596 (1970).
[58] K. Alvi, Phys. Rev. D **61**, 124013 (2000).
[59] K. S. Thorne and J. B. Hartle, Phys. Rev. D **31**, 1815 (1985).
[60] L. E. Kidder, Phys. Rev. D **52**, 821 (1995).
[61] E. Schnetter, B. Krishnan, and F. Beyer, Phys. Rev. D **74**, 024028 (2006).